Electronic Supplementary Information

for

Isomeric diazapyrene-thiophene Conjugated Systems: Synthesis, Characterization, and Transport Properties

Honglei Li,[ab] Guodong Zhao,[c] Qingxin Tang, [c] Hongkun Tian,*[ab] and Lixiang Wang [ab]

[a.] State Key Laboratory of Polymer Physics and Chemistry, Changchun Institute of Applied Chemistry, Chinese Academy of Sciences, Changchun, 130022, P. R. China.

[b.] School of Applied Chemistry and Engineering, University of Science and Technology of China, Hefei, Anhui, 230026, China.

[c.] Center for Advanced Optoelectronic Functional Materials Research and Key Lab of UV-Emitting Materials and Technology of Ministry of Education, Northeast Normal University, Changchun, 130024 P. R. China.

1. Instruments, OFETs fabrication and measurements

Instruments. ^{1}H NMR and ^{13}C NMR (25 ^{o}C, $CDCl_3$ with tetramethylsilane as internal standard or 110 ^{o}C, 1,1,2,2-tetrachloroethane-d^2($C_2D_2Cl_4$)) spectra of all compounds were measured by a Bruker AV 400-MHz or 500-MHz spectrometer. Matrix-assisted laser desorption ionization time-of-flight (MALDI-TOF) mass spectra were recorded in reflection mode on a Brucker/AutoflexIII mass spectrometer. Elemental analysis was performed on a VarioEL elemental analyzer. Thermogravimetric analysis (TGA) was carried out on a TA Q50 thermogravimetric analyzer with the heating rate of 10 °C min^{-1} at a nitrogen flow. Differential scanning calorimetry (DSC) was conducted on a TA Q2000 instrument with a heating/cooling rate of 10 ^{o}C min^{-1} under nitrogen. UV-*vis* absorption spectra were recorded on a Shimadzu UV3600-plus spectrometer. Cyclic voltamograms (CV, scan rate: 100 mV s^{-1}) were measured using a CHI660a electrochemical analyzer with a three-electrode cell with tetrabutylammonium hexafluorophosphate (Bu_4NPF_6, 0.1 mol L^{-1}) as the supporting electrolyte in anhydrous dichloromethane solutions. The CV cell consisted of a Pt disc working electrode, a Pt wire counter electrode, and a standard calomel reference electrode. For calibration, the redox half-wave potential of ferrocene/ferrocenium (Fc/Fc^{+}) was measured under the same conditions, which was 0.43 eV versus SCE. The highest occupied molecular orbital (HOMO) energy levels were calculated according to the equations $E_{HOMO} = -(4.80 + E_{onset}^{ox})$ eV, in which E_{onset}^{ox} represent oxidation onsets. The out-of-plane and in-plane XRD patterns were recorded with a Rigaku Smart Lab instrument with Cu-Ka radiation (λ = 1.54056 Å).The selected voltage and current were 40 kV and 35 mA, respectively. Atomic force microscopy (AFM) measurements were carried out in tapping mode on a Bruker MultiMode 8 atomic force microscope. Polarized optical microscopy was performed using Carl Zeiss Microlmaging GmbH Axio Imager A2m.

Theoretical calculations. All calculations for molecular orbitals and frontier orbital levels were performed using Gaussian 09 at the B3LYP/6-31G (d,p) level.[1] The alkyl chains of the model polymers were replaced with methyl chains. To investigate the hole transport properties, the transfer integrals [2] between the HOMOs of adjacent molecules were calculated based on the crystal geometries using PW91 exchange and PW91 correlation functionals with the 6-31G* basis set.[3,4]

Materials and reagents. All commercially available chemicals were used without further purification unless otherwise stated. Tetrahydrofuran (THF) and toluene (Tol) were dried using sodium before use. All reactions were carried out under Ar atmosphere. 5-Octyl-5-[4,4,5,5-tetramethyl-1,3,2-dioxaborolanyl]-2,2-bithiophene was synthesized according to previous reported precedure.[5-8]

OFET fabrication and measurements. The charge transport properties of the molecules were characterized by using top gate/bottom contact (TG/BC) OFETs. Highly n-doped silicon wafers covered with a 200 nm thick thermally grown SiO_2 layer, which are commercially available and have flat and smooth surface, were used as substrates. The SiO_2/Si substrates were modified with octadecyltrimethoxysilane

(OTMS) monolayer according to the literature method.[9] Semiconductor layers (~30 nm thick) were vacuum deposited onto the OTMS modified substrates (Sub_{OTMS}) at a rate of 0.5–1 Å s^{-1} under a pressure of 10^{-4} Pa at an optimized substrate temperature. Au source and drain electrodes (40 nm) were vacuum deposited onto the semiconductor layer through a shadow mask. The channel length was 200 μm and the channel width was 1 mm. The electrical measurements were performed with a Keysight B1500A and a probe stage (PEH-4 from EveryBeing Limited Company) in the dark and under ambient conditions at a scan rate of 1 V s^{-1}. Field-effect mobility in saturation regime was calculated by using the equation: $I^{sat}_{DS} = (\mu C_i W/2L)(V_{GS}-V_{th})^2$, in which I_{DS} is the drain-source current, μ is the field effect mobility, C_i (17.3 nF cm^{-2}) is the capacitance per unit area of the dielectric layer, V_{GS} and V_{th} are the gate voltage and threshold voltage, respectively.

SC-OFET fabrication. On the cleaned SiO_2/Si wafer modified by OTMS was put a drop of the solution containing the **3,8-PyNN-TT** (0.5 mg mL^{-1}). The solvent was controlled to slowly evaporate in several days. Then the single crystals in micrometer scale may grow on the substrates. Different solvents (toluene, chlorobenzene and chloroform) were used for crystal preparation, and the best quality crystals were selected on a Micromanipulator station coupled with an optical microscope to further fabricate the transistor device. Two pieces of the Au films, approximately 150 μm × 30 μm, were glued onto the selected single crystals via the electrostatic forces with the help of the mechanical probes in the Micromanipulator. The above mentioned Au films were prepared as follow: firstly, a patterned Au thin film with a thickness around 100 nm was pre-deposited on a Si wafer by thermal evaporation with a copper mask. Then, two small pieces of the Au films with desired sizes were peeled off from the Si substrate with the tip of the mechanical probe and transferred onto the single crystals as source and drain electrodes. The Si substrate functioned as the gate electrode.

2. Synthetic procedures

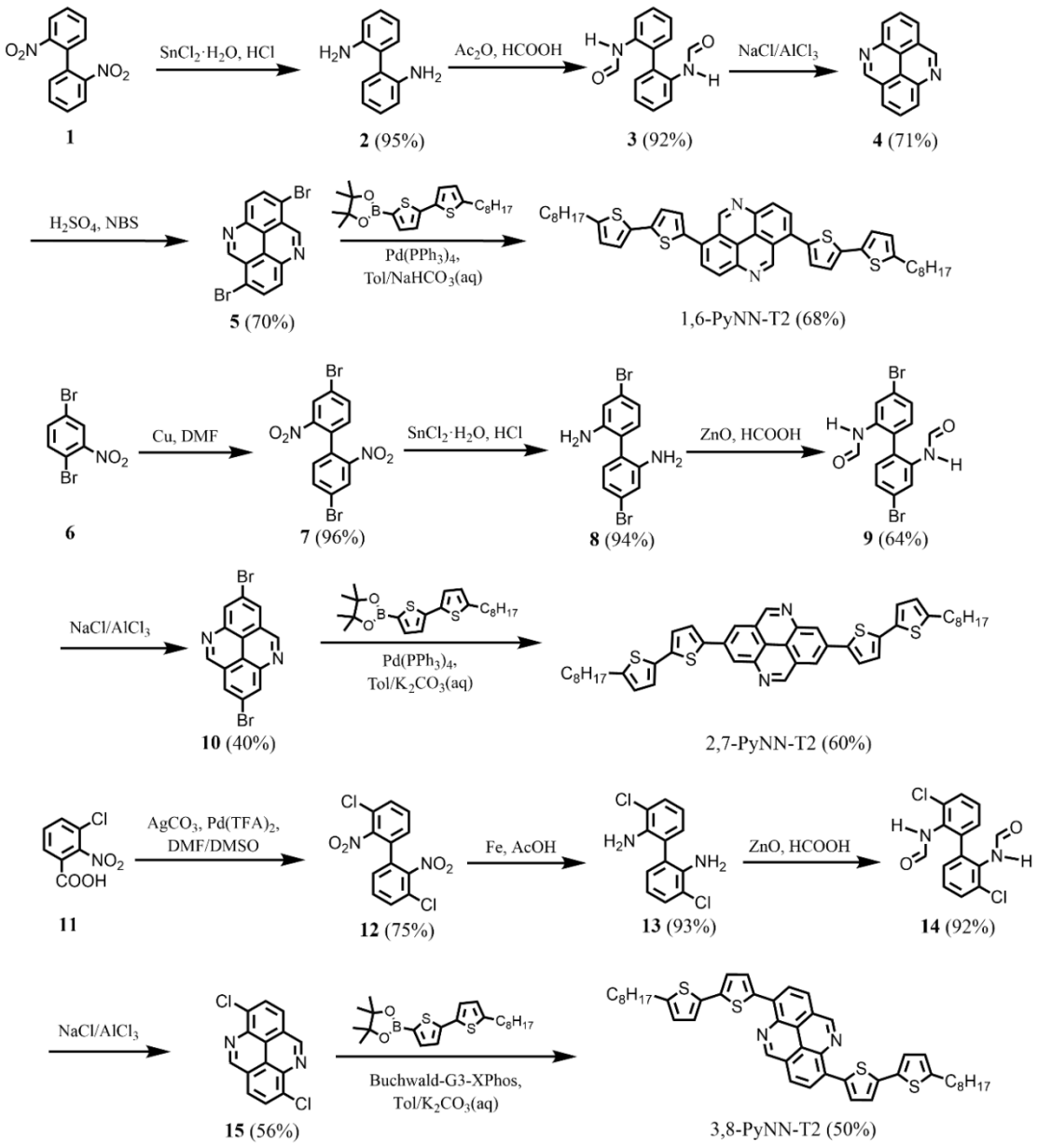

Scheme S1. Synthetic Routes to 1,6-PyNN-T2, 2,7-PyNN-T2, and 3,8-PyNN-T2

2,2'-Diaminobiphenyl (2)

The solution of 2,2'-dinitrobiphenyl (**1**,15.00 g, 61.35 mmol) and $SnCl_2 \cdot H_2O$ (124.54 g, 552.15 mmol) in concentrated HCl (225 mL) was refluxed at 100 ^oC for 2 h in the air. The reaction was then quenched by aqueous NaOH solution at this temperature. The yellow solid was formed in the mixture, which was purified by filtration and washed with water. After dried in the vacuum line, compound **2** were obtained as a yellow solid (10.74 g, 95%). ^1H NMR (500 MHz, $CDCl_3$, 293 K): δ (ppm) 7.17 (t, *J* =

7.5 Hz, 2H), 7.12 (d, *J* = 7.5 Hz, 2H), 6.87 (t, *J* = 7.5 Hz, 2H), 6.82 (d, *J* = 7.5 Hz, 2H), 3.82 (*brs*, 4H). ^{13}C NMR (125 MHz, $CDCl_3$, 293 K): δ (ppm) 144.05, 131.05, 128.81, 0124.62, 118.85, 115.60.

N,N'-(Biphenyl-2,2'-diyl)diformamid (3)

Based on procedures reported in the literature[10], acetic anhydride (27.45 mL, 293.45 mmol) was added to formic acid (10.95 mL, 293.45 mmol) and the mixture was stirred at 55 ^{o}C for 2 h. The reaction mixture was then added dropwise to a solution of diamine **2** (10.74 g, 58.29 mmol) in THF (180 mL) at 0 ^{o}C. After warming to room temperature (RT), stirring was continued for 2 h. Afterwards the reaction was quenched by addition of saturated aqueous $NaHCO_3$ solution (500 mL). The aqueous layer was extracted with EtOAc (3 x 300 mL) and the combined organic layers were dried over $MgSO_4$. After removing the solvent *in vacuo*, the crude product of **3** was obtained as a white solid (12.88 g, 92%) and used without purification.

pyrido[2,3,4,5-lmn]phenanthridine (4)

Based on procedures reported in the literature[10], **3** (12.88 g, 53.63 mmol) was added to a molten mixture of NaCl (50.15 g, 858.08 mmol) and $AlCl_3$ (228.83 g, 1.72 mol,) at 100 °C. The mixture was stirred at 230 ^{o}C for 8 h. After cooling to 100 ^{o}C, the mixture was added to an ice/water mixture (500 mL). The mixture was alkalized and extracted with EtOAc (3 x 1 L). The combined organic layers were washed with brine (500 mL) and dried over $MgSO_4$. After removing the solvent *in vacuo*, the residue was purified by chromatography on a silica gel column, eluting with dichloromethane (DCM)/ methanol (v/v, 15/1) to afford diazapyrene **4** as an yellow solid (7.76 g, 71%). ^{1}H NMR (500 MHz, $CDCl_3$, 293 K): δ (ppm) 9.74 (s, 2H), 8.76 (d, *J* = 8.0 Hz, 2H), 8.47 (d, *J* = 8.0 Hz, 2H), 8.33 (t, *J* = 8.0 Hz, 2H). ^{13}C NMR (125 MHz, $CDCl_3$, 293 K): δ (ppm) 154.49, 141.78, 129.97, 128.77, 125.57, 125.21, 120.42.

1,6-dibromopyrido[2,3,4,5-lmn]phenanthridine (5)

A mixture of diazapyrene **4** (2.04 g, 10 mmol) with NBS (4.63g, 26 mmol) in 10 mL of 98% H_2SO_4 was stired for 12 h at 20 ^{o}C.[11] After the reaction mixture was poured into an ice/water mixture (50 mL), the aqueous mixture was made alkaline to pH 10 with aqueous solution of concentrated ammonia, and the precipitate was extracted with chloroform. The extract was dried with $MgSO_4$, the solvent was evaporated, and recrystallization using chloroform yields a white solid **5** (1.59 g, 70%). ^{1}H NMR (500 MHz, $CDCl_3$, 293 K): δ (ppm) 9.97 (s, 2H), 8.64 (d, *J* = 8.5 Hz, 2H), 8.50 (d, *J* = 8.5 Hz, 2H). ^{13}C NMR (100 MHz, $C_2D_2Cl_4$, 383 K): δ (ppm) 153.60, 141.71, 133.68, 131.23, 123.42, 121.29, 120.97.

1,6-bis(5'-octyl-[2,2'-bithiophen]-5-yl)pyrido[2,3,4,5-lmn]phenanthridine (1,6-PyNN-T2)

A mixture of **4** (1.59 g, 4.40 mmol), 5-octyl-5′-[4,4,5,5-tetramethyl-1,3,2 -dioxaborolanyl]-2,2′-bithiophene (4.09 g, 10.12 mmol), K_2CO_3 (4.38 g, 31.7 mmol), toluene (46 mL), and H_2O (23 mL) was degassed before and after $Pd(PPh_3)_4$ (0.20 g, 0.18 mmol) was added. The mixture was heated to 100 ^{o}C and stirred under Ar atmosphere for 24 h. After reaction, the crude residue was precipitated in methanol and then further purified by Soxhlet extractions with acetone, hexane and chloroform during 24 hours each. The chloroform fraction was collected and concentrated under

reduced pressure, and then vacuum sublimation twice. Orange product **1,6-PyNN-T2** was obtained (2.27g, 68%). ^{1}H NMR (500 MHz, $CDCl_3$, 293 K): δ (ppm) 10.09 (s, 2H), 8.62 (d, *J* = 8.0Hz, 2H), 8.32 (d, *J* = 8.5 Hz, 2H), 7.39 (d, *J* = 3.5 Hz, 2H), 7.28 (d, *J* = 4.0 Hz, 2H), 7.12 (d, *J* = 3.5 Hz, 2H), 6.75 (d, *J* = 3.5 Hz, 2H), 2.85 (t, *J* = 7.5 Hz, 4H), 1.29-1.73 (m, 24H), 0.91 (t, *J* = 7.0 Hz, 6H). ^{13}C NMR (125 MHz, $CDCl_3$, 293 K): δ (ppm) 152.70, 146.37, 141.14, 140.71, 137.49, 134.08, 131.84, 130.94, 129.87, 129.64, 125.04, 124.04, 123.91, 122.19, 121.15, 31.87, 31.83, 30.24, 29.35, 29.24, 29.11, 22.67, 14.12. Elem. anal. calcd for $C_{46}H_{48}N_2S_4$: C, 72.97; H, 6.39; N, 3.70; S, 16.94; found: C, 73.31; H, 6.44; N, 3.75; S, 17.01; MS (MALDI-TOF, calcd: 756.2700): found: 756.2656.

4,4'-dibromo-2,2'-dinitro-1,1'-biphenyl (7)

Based on procedures reported in the literature,[12] to a solution of **5** (10.00 g, 35.60 mmol) in DMF (140 mL), copper powder (5 g, 78.13 mmol) was added. The mixture was stirred under reflux in Ar atmosphere for 3 h. After the mixture was cooled to RT, the precipitate was filtered and DMF was evaporated under reduced pressure. The residue was dissolved in DCM and washed with saturated brine. The combined organic phase was dried over anhydrous $MgSO_4$ and concentrated. After the residue was recrystallized in ethanol, the product **6** was obtained as a yellow solid (6.92 g, 96%). ^{1}H NMR (500 MHz, $CDCl_3$, 293 K): δ (ppm) 8.38 (d, *J* = 2.0 Hz, 2H), 7.84 (dd, *J* = 8.5 Hz, *J* = 2.0Hz, 2H), 7.17 (d, *J* = 8.0 Hz, 2H). ^{13}C NMR (125 MHz, $CDCl_3$, 293 K): δ (ppm) 147.38, 136.65, 132.04, 131.99, 128.07, 122.92.

4,4'-dibromo-[1,1'-biphenyl]-2,2'-diamine (8)

The procedure was the same as the synthesis of compound **2.** compound **8** was obtained as a white solid with a yield of 94%. ^{1}H NMR (500 MHz, $CDCl_3$, 293 K): δ (ppm) 6.92 (m, 6H), 3.74 (brs, 4H). ^{13}C NMR (125 MHz, $CDCl_3$, 293 K): δ (ppm) 145.38, 132.25, 122.70, 122.05, 121.68, 118.11.

N,N'-(4,4'-dibromo-[1,1'-biphenyl]-2,2'-diyl)diformamide (9)

Based on procedures reported in the literature,[13] to a mixture of HCO_2H (10 mL, 264.76 mmol) and ZnO (1.32 g, 16.17 mmol) was added **8** (5.53 g, 16.17 mmol), and then the reaction mixture was heated in an oil bath at 70 ^{o}C and stirred with a magnetic stirrer. The progress of the reaction was monitored by thin layer chromatography (TLC). After the reaction was complete, DCM was added to the reaction mixture, and ZnO was removed by filtration. The organic solvent was then washed with H_2O and a saturated solution of $NaHCO_3$ and dried over anhydrous Na_2SO_4. After removal of the solvent, the pure product was obtained. This was further purified by recrystallization with $CHCl_3$. Compound **9** was obtained as a white solid (4.12 g, 64%) and used without purification. ^{1}H NMR (500 MHz, $CDCl_3$, 293 K): δ (ppm) 8.59 (s, 2H), 7.23 (s, 2H), 7.43 (d, *J* = 8.0 Hz, 2H), 7.07 (d, *J* = 8.0 Hz, 2H), 6.87 (brs, 2H). ^{13}C NMR (100 MHz, $C_2D_2Cl_4$, 383 K): δ (ppm) 159.62, 136.15, 131.94, 128.95, 126.39, 123.86.

2,7-dibromopyrido[2,3,4,5-lmn]phenanthridine (10)

The procedure was the same as the synthesis of compound **4.** Compound **10** was obtained as a pale yellow solid with a yield of 40%. ^{1}H NMR (500 MHz, $CDCl_3$, 293

K): δ (ppm) 9.63 (s, 2H), 8.82 (s, 2H), 8.55 (s, 2H). ^{13}C NMR (100 MHz, $C_2D_2Cl_4$, 383 K): δ (ppm) 154.35, 143.04, 133.45, 128.70, 126.15, 123.02, 118.94.

2,7-bis(5'-octyl-[2,2'-bithiophen]-5-yl)pyrido[2,3,4,5-lmn]phenanthridine (2,7-PyNN-T2)

The procedure was the same as the synthesis of compound **1,6-PyNN-T2.** Compound **2,7-PyNN-T2** was obtained as a yellow solid with a yield of 60%. ^{1}H NMR (500 MHz, $CDCl_3$, 293 K): δ (ppm) 9.66 (s, 2H), 8.82 (d, *J* = 1.5 Hz, 2H), 8.50 (d, *J* = 1.5 Hz, 2H), 7.54 (d, *J* = 1.5 Hz, 2H), 7.15 (d, *J* = 3.5 Hz, 2H), 7.08 (d, *J* = 3.5 Hz, 2H), 6.73 (d, *J* = 3.5 Hz, 2H), 2.83 (t, *J* = 7.5 Hz, 4H), 1.28-1.71 (m, 24H), 0.91 (t, *J* = 7.0 Hz, 6H). ^{13}C NMR (100 MHz, $C_2D_2Cl_4$, 383 K): δ (ppm) 154.78, 146.36, 142.17, 141.36, 139.44, 135.10, 134.51, 126.56, 125.49, 125.45, 124.98, 124.33, 124.10, 122.05, 119.13, 31.89, 31.48, 30.31, 29.35, 29.24, 29.20, 22.62, 13.97. Elem. anal. calcd for $C_{46}H_{48}N_2S_4$: C, 72.97; H, 6.39; N, 3.70; S, 16.94; found: C, 73.31; H, 6.30; N, 3.81; S, 17.10; MS (MALDI-TOF, calcd: 756.2700): found: 756.2675.

3,3'-dichloro-2,2'-dinitro-1,1'-biphenyl (12)

A suspension of **11** (18.14 g, 90 mmol), Ag_2CO_3 (24.82 g, 90 mmol) and $Pd(TFA)_2$ (2.15 g, 6.48 mmol) in 600 mL of DMF/DMSO (95/5, v/v) was stirred at 120 ºC for 16 h.[14] After this time, the reaction mixture was cooled down to RT and filtered through a plug of silica gel with EtOAc. The filtrate was washed with a saturated solution of $NaHCO_3$, brine and the organic layer was evaporated to dryness under reduced pressure. Compound **12** was obtained as a white solid (10.5 g, 75%) and used without purification. ^{1}H NMR (500 MHz, $CDCl_3$, 293 K): δ (ppm) 7.62 (dd, *J* = 8.5 Hz, *J* = 1.5 Hz, 2H), 7.50 (t, *J* = 8.5 Hz, 2H), 7.31 (dd, *J* = 8.5 Hz, *J* = 1.5 Hz, 2H). ^{13}C NMR (125 MHz, $CDCl_3$, 293 K): δ (ppm) 148.85, 131.72, 131.00, 129.23, 128.76, 126.17.

3,3'-dichloro-[1,1'-biphenyl]-2,2'-diamine (13)

The mixture of glacial acetic acid (300 mL), **12** (10.5 g, 33.53 mmol), and iron powder (26.22 g, 469 mmol) was heated at 80 ^{o}C for 12 h. After cooling to RT, the iron powder was removed by filtration. After a large amount of water was added to the filtrate, solid appeared in the solution. The crude product was collected by filtration and purified by silica gel column chromatography with DCM as the eluent to yield compound **13** (7.86 g, 93%).^{1}H NMR (500 MHz, $CDCl_3$, 293 K): δ (ppm) 7.31 (dd, *J* = 8.0 Hz, *J* = 1.5 Hz, 2H), 7.02 (dd, *J* = 7.5 Hz, *J* = 1.5 Hz, 2H), 6.77 (t, *J* = 7.5 Hz, 2H), 3.95 (brs, 4H). ^{13}C NMR (125 MHz, $CDCl_3$, 293 K): δ (ppm) 140.84, 129.29, 129.22, 124.68, 119.76, 118.62.

N,N'-(3,3'-dichloro-[1,1'-biphenyl]-2,2'-diyl)diformamide (14)

The procedure was the same as the synthesis of compound **9.** Compound **14** was obtained as a white solid with a yield of 92% and used without purification.

3,8-dichloropyrido[2,3,4,5-lmn]phenanthridine (15)

The procedure was the same as the synthesis of compound **4.** Compound **15** was obtained as a white solid with a yield of 56%. ^{1}H NMR (500 MHz, $CDCl_3$, 293 K): δ (ppm) 9.76 (s, 2H), 8.39 (d, *J* = 8.0 Hz, 2H), 8.38 (d, *J* = 8.0 Hz, 2H). ^{13}C NMR (125

MHz, $CDCl_3$, 293 K): δ (ppm) 154.65, 138.25, 135.75, 130.52, 126.46, 123.88, 128.28.

3,8-bis(5'-octyl-[2,2'-bithiophen]-5-yl)pyrido[2,3,4,5-lmn]phenanthridine (3,8-PyNN-T2)

A mixture of **15** (1.31 g, 4.83 mmol), 5-octyl-5′-[4,4,5,5-tetramethyl-1,3,2 -dioxaborolanyl]-2,2′-bithiophene (4.49 g, 11.11 mmol), K_2CO_3 (4.81 g, 34.8 mmol), toluene (48 mL), and H_2O (24 mL) was degassed before and after Buchwald-G3-XPhos (0.16 g, 0.19 mmol) was added. The mixture was heated to reflux and stirred under Ar atmosphere for 24 h. After reaction, the crude residue was precipitated in methanol and then further purified by Soxhlet extractions with acetone, hexane and chloroform during 24 hours each. The chloroform fraction was collected and concentrated under reduced pressure, and then vacuum sublimation. Orange product **3,8-PyNN-TT** was obtained (2.0 g, 55%). ^{1}H NMR (400 MHz, $C_2D_2Cl_4$, 383 K): δ (ppm) 9.76 (s, 2H), 8.68 (d, *J* = 8.4 Hz, 2H), 8.39 (d, *J* = 8.4 Hz, 2H), 8.12 (d, *J* = 4.0 Hz, 2H), 7.35 (d, *J* = 4.0 Hz, 2H), 7.29 (d, *J* = 3.2 Hz, 2H), 6.86 (d, *J* = 3.2Hz, 2H), 2.98 (t, *J* = 7.2 Hz, 4H), 1.40-1.88 (m, 24H), 1.02 (m, 6H). ^{13}C NMR (100 MHz, $C_2D_2Cl_4$, 383 K): δ (ppm) 152.24, 146.24, 142.82, 138.19, 137.66, 135.32, 133.49, 129.08, 126.59, 125.04, 124.82, 123.99, 123.77, 123.16, 121.66, 31.90, 31.56, 30.38, 29.37, 29.25, 29.21, 22.63, 13.98. Elem. anal. calcd for $C_{46}H_{48}N_2S_4$: C, 72.97; H, 6.39; N, 3.70; S, 16.94; found: C, 73.15; H, 6.40; N, 3.76; S, 17.17; MS (MALDI-TOF, calcd: 756.2700): found: 756.2669.

3. ^{1}H and ^{13}C NMR spectra

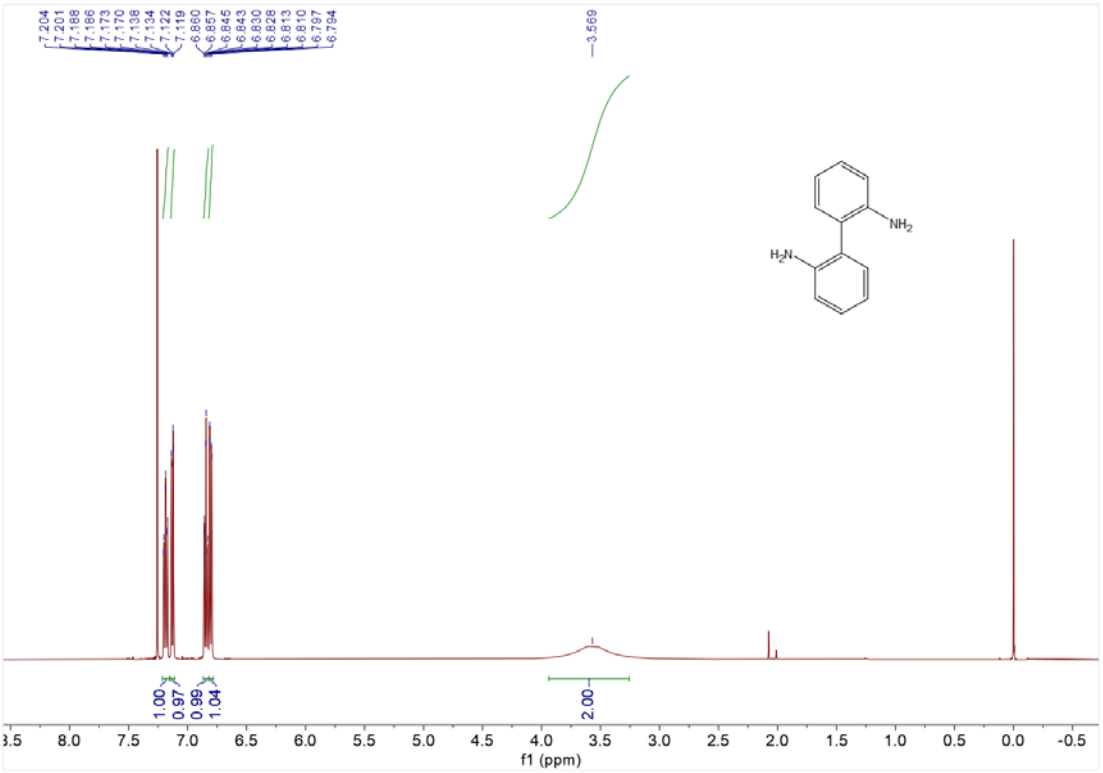

Figure S1. ^{1}H NMR spectrum of **2**.

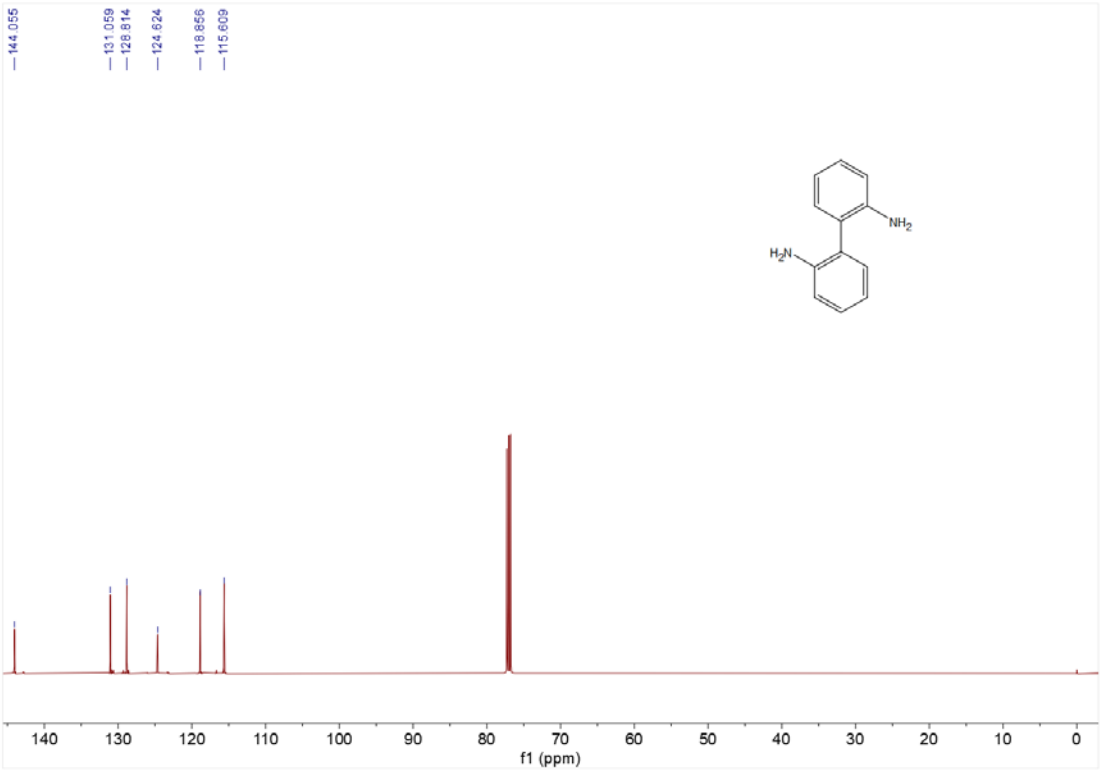

Figure S2. ^{13}C NMR spectrum of **2**.

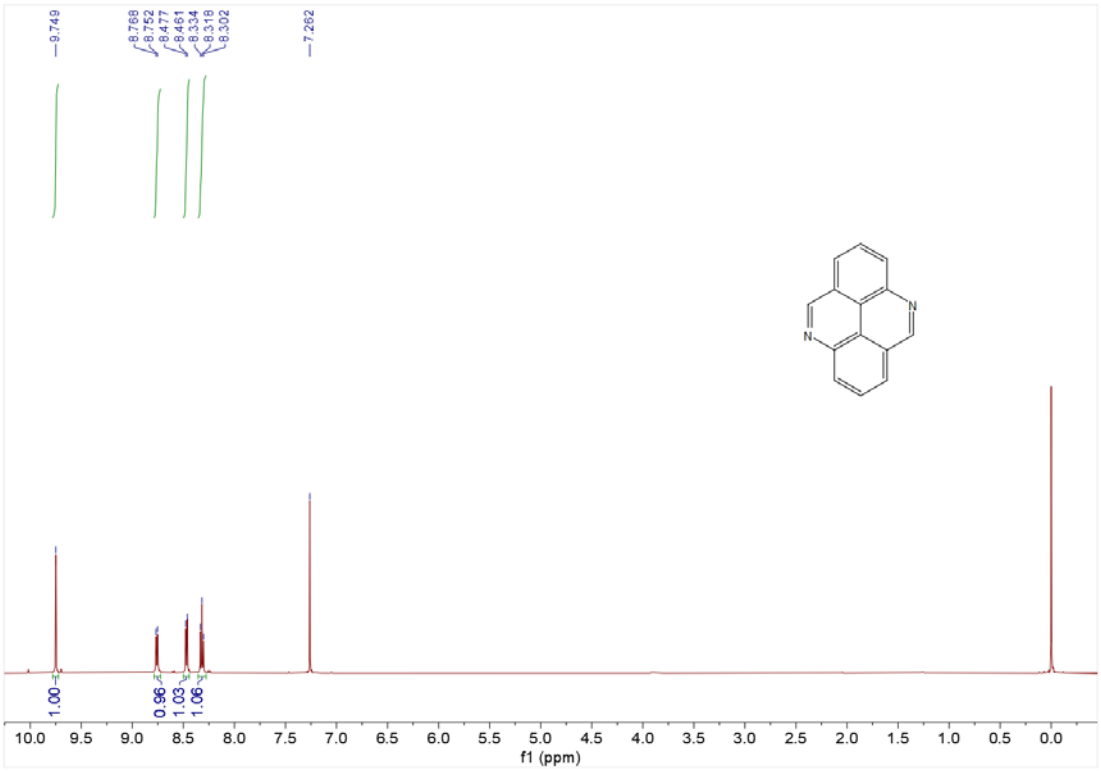

Figure S3. ^{1}H NMR spectrum of **4**.

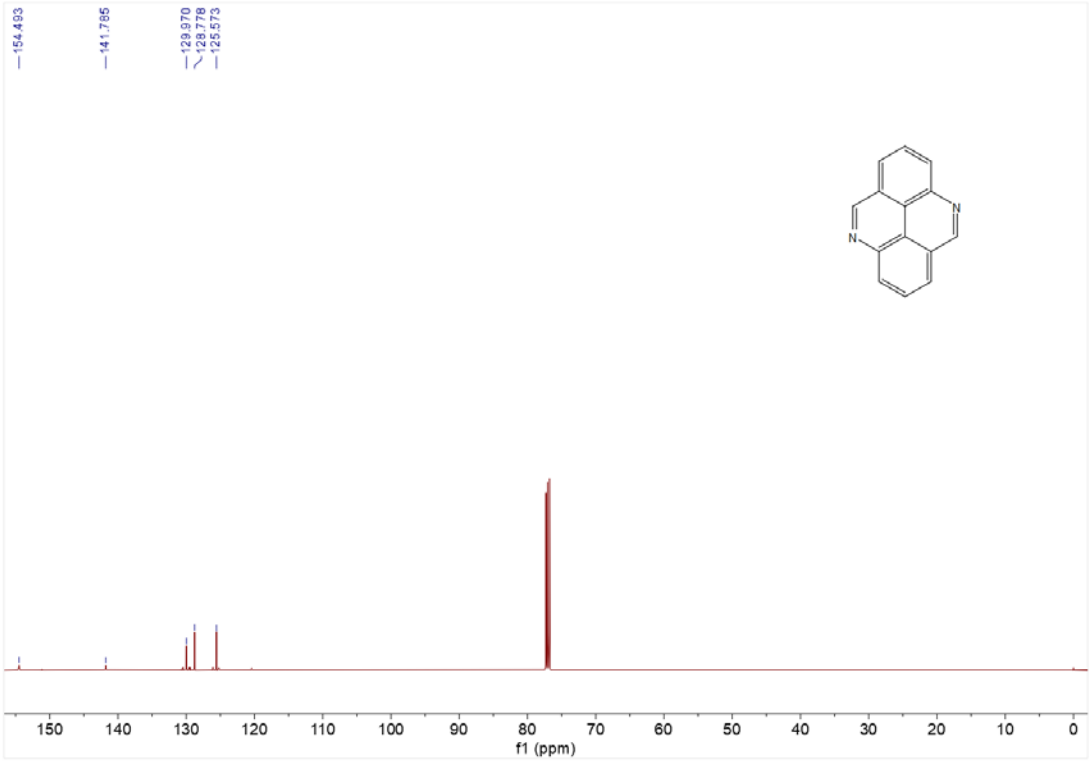

Figure S4. ^{13}C NMR spectrum of **4**.

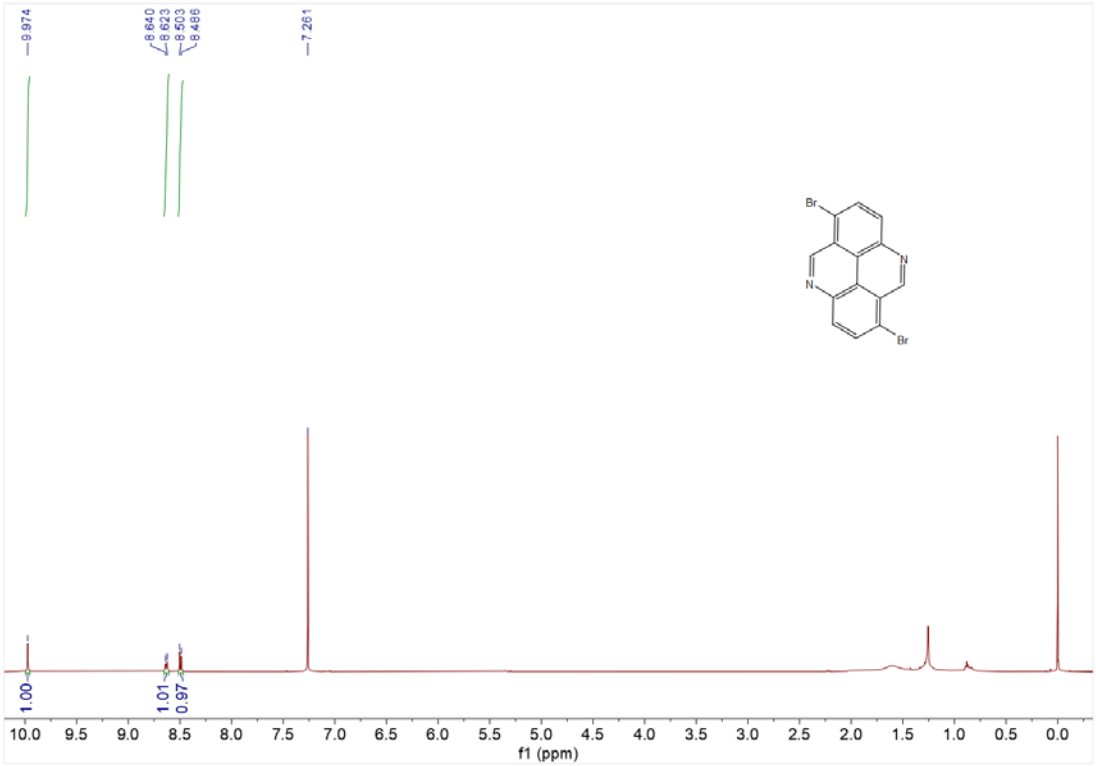

Figure S5. ^{1}H NMR spectrum of **5**.

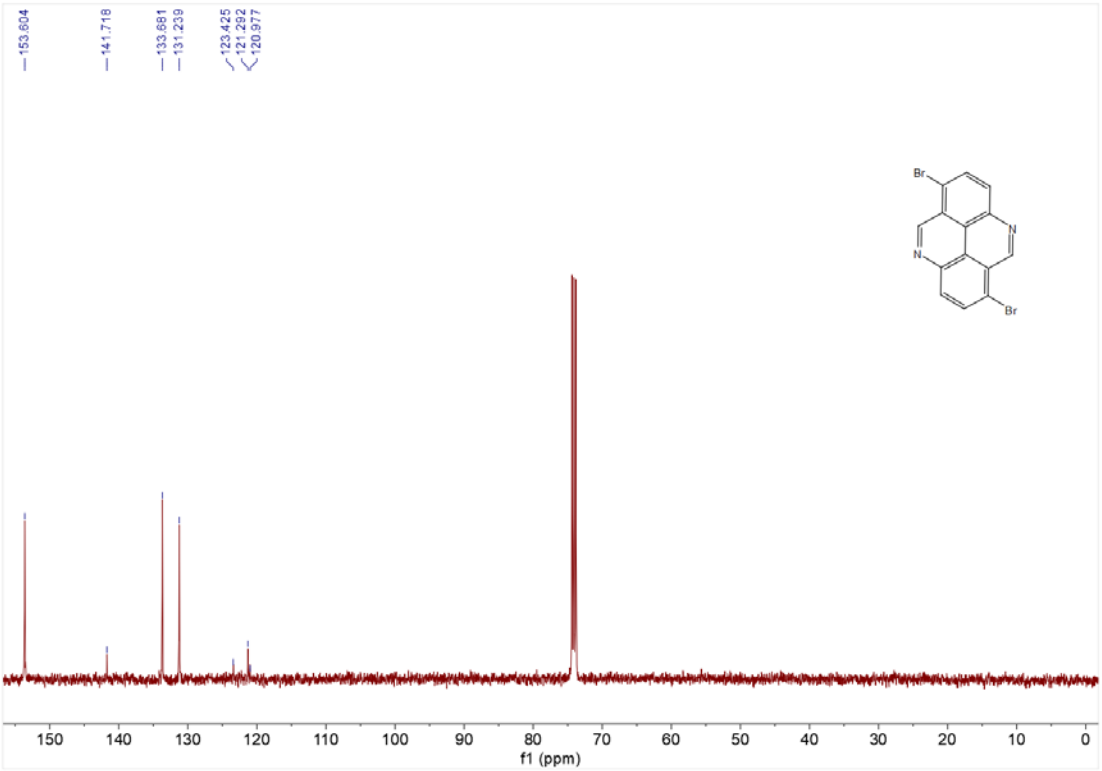

Figure S6. ^{13}C NMR spectrum of **5**.

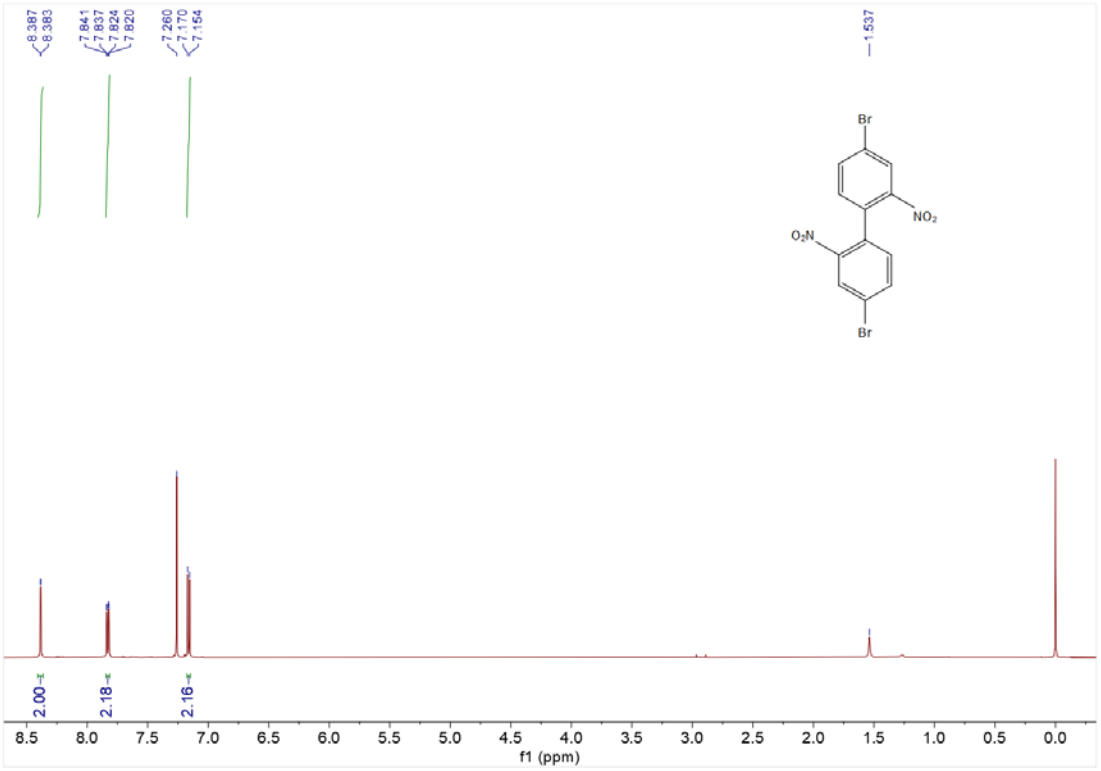

Figure S7. ^{1}H NMR spectrum of **7**.

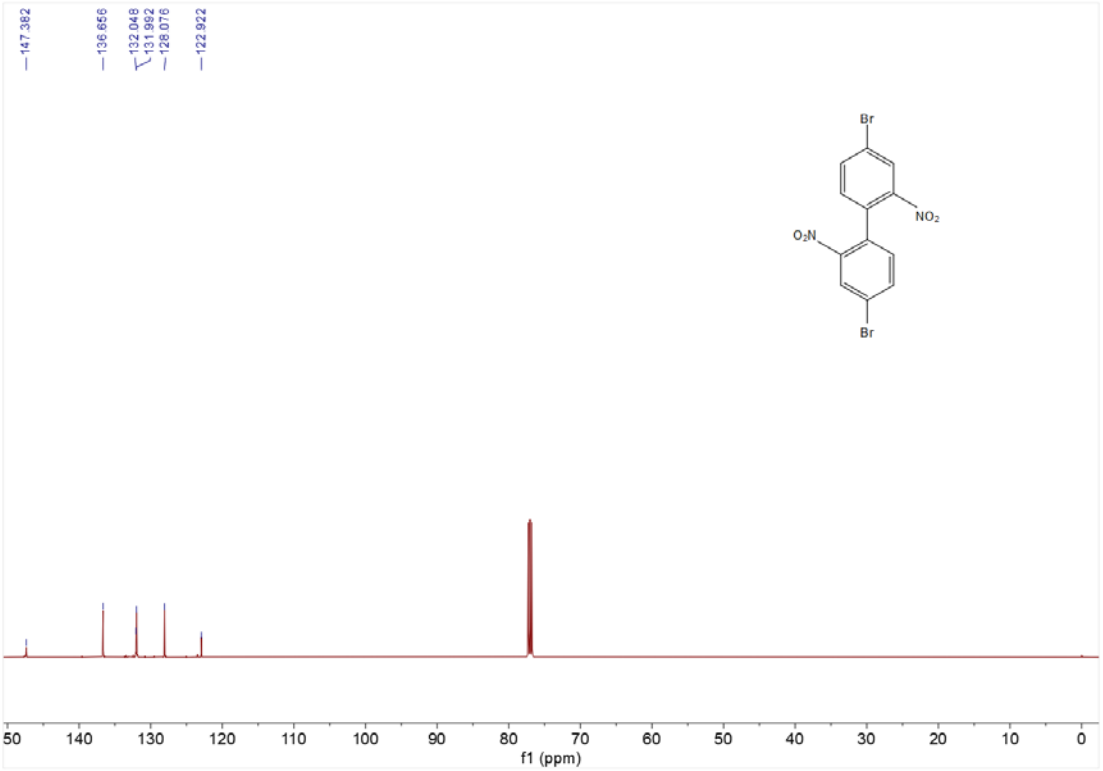

Figure S8. ^{13}C NMR spectrum of **7**.

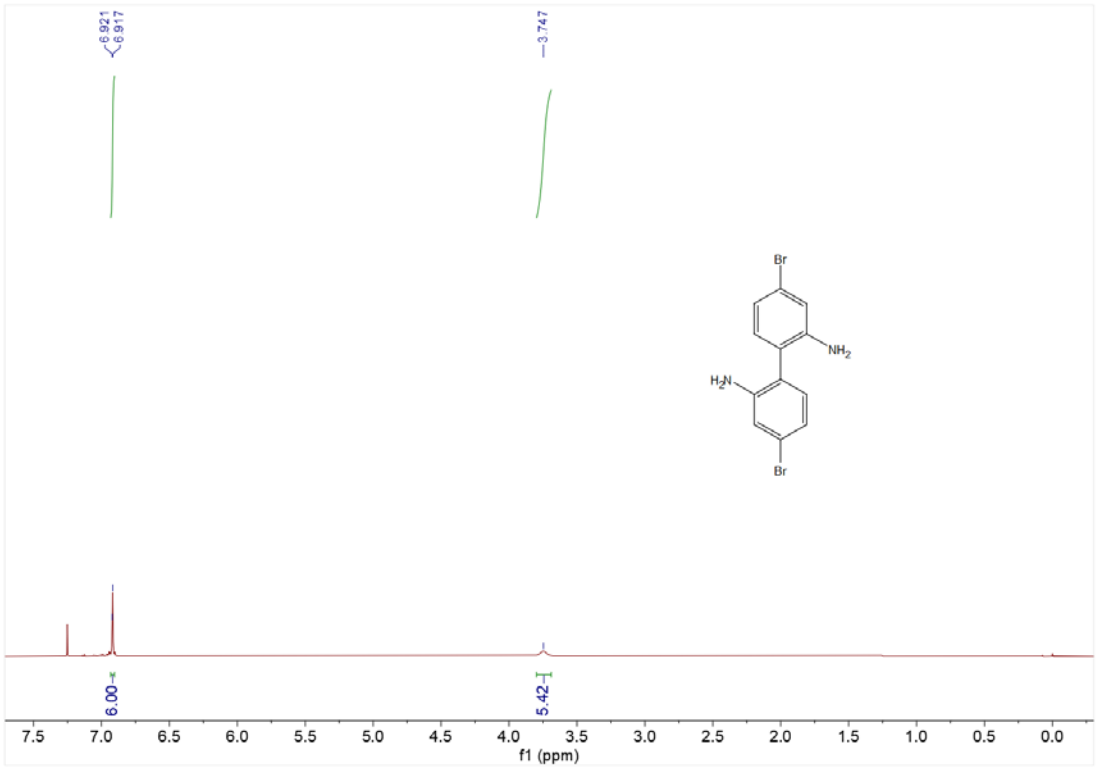

Figure S9. ^{1}H NMR spectrum of **8**.

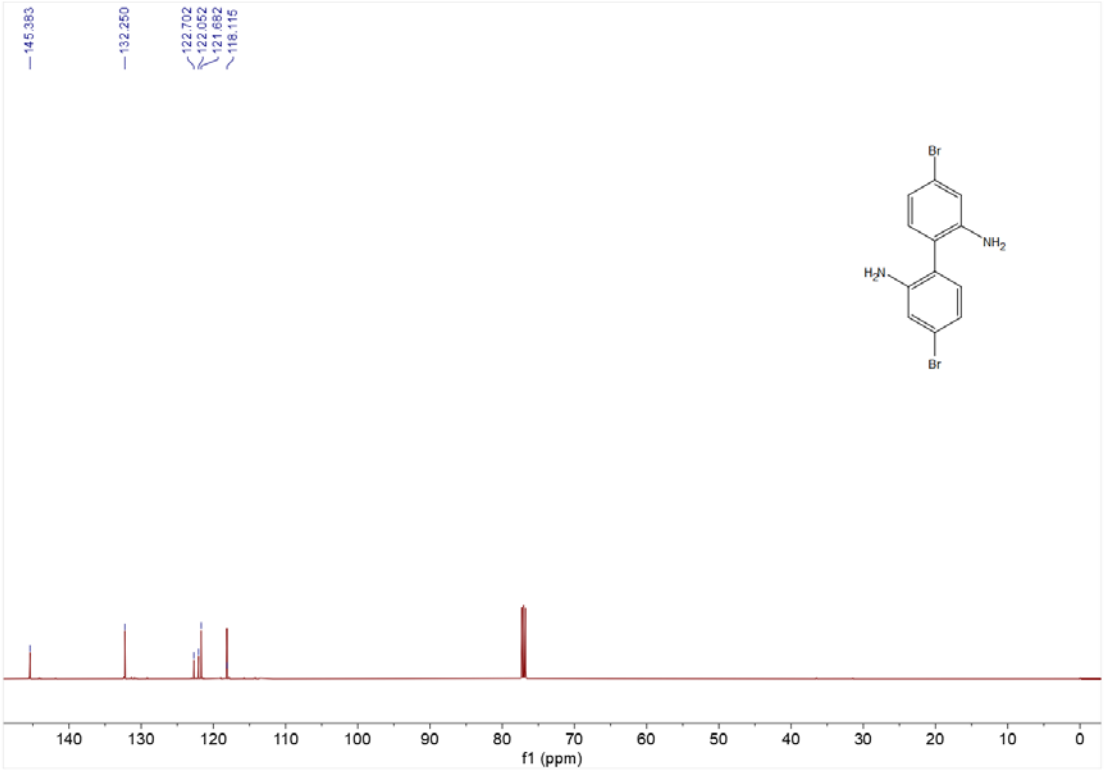

Figure S10. ^{13}C NMR spectrum of **8**.

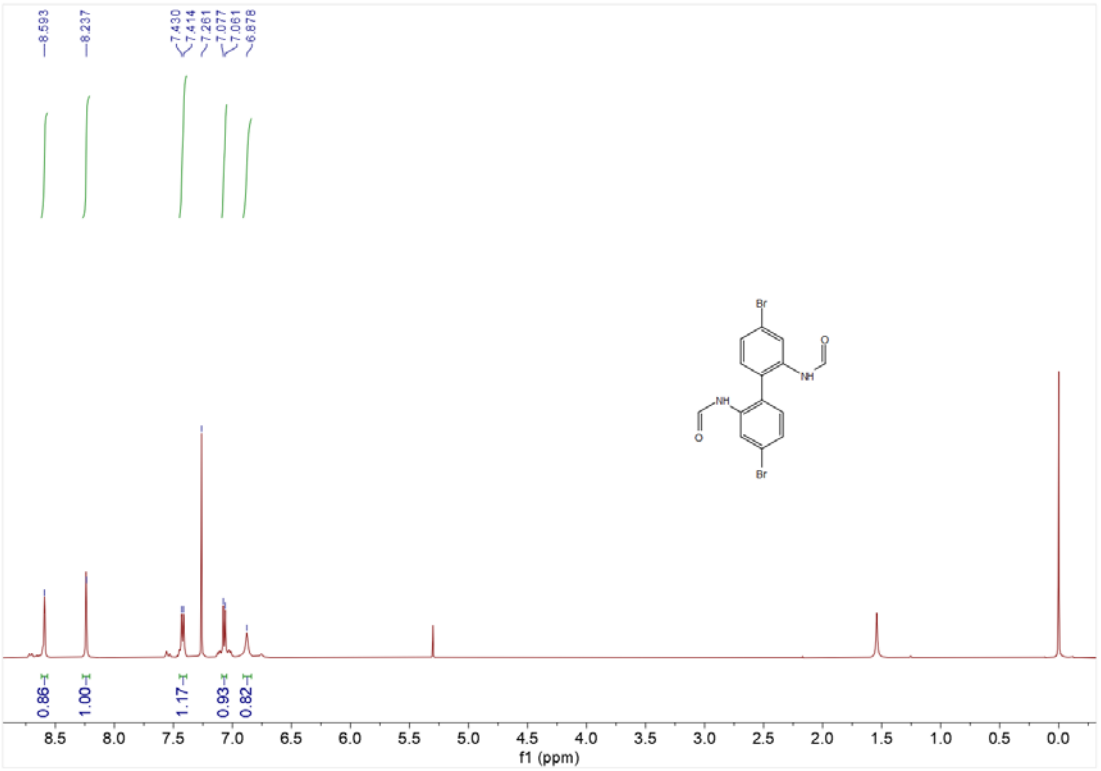

Figure S11. ^{1}H NMR spectrum of **9**.

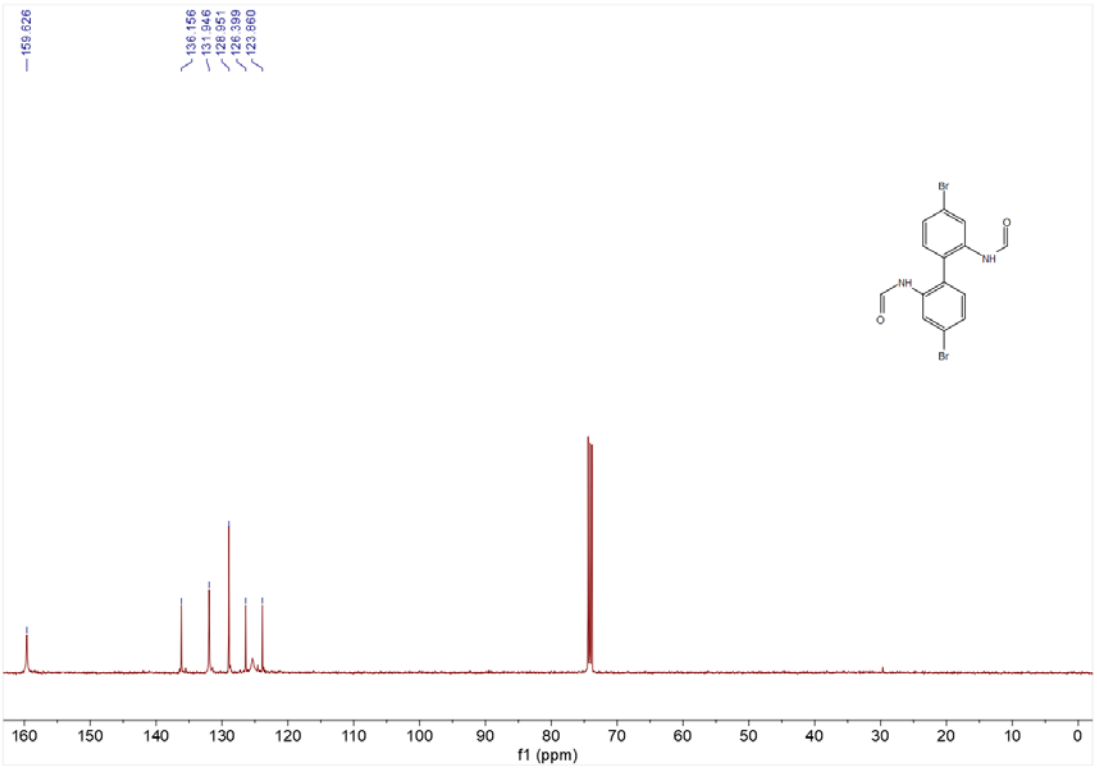

Figure S12. ^{13}C NMR spectrum of **9**.

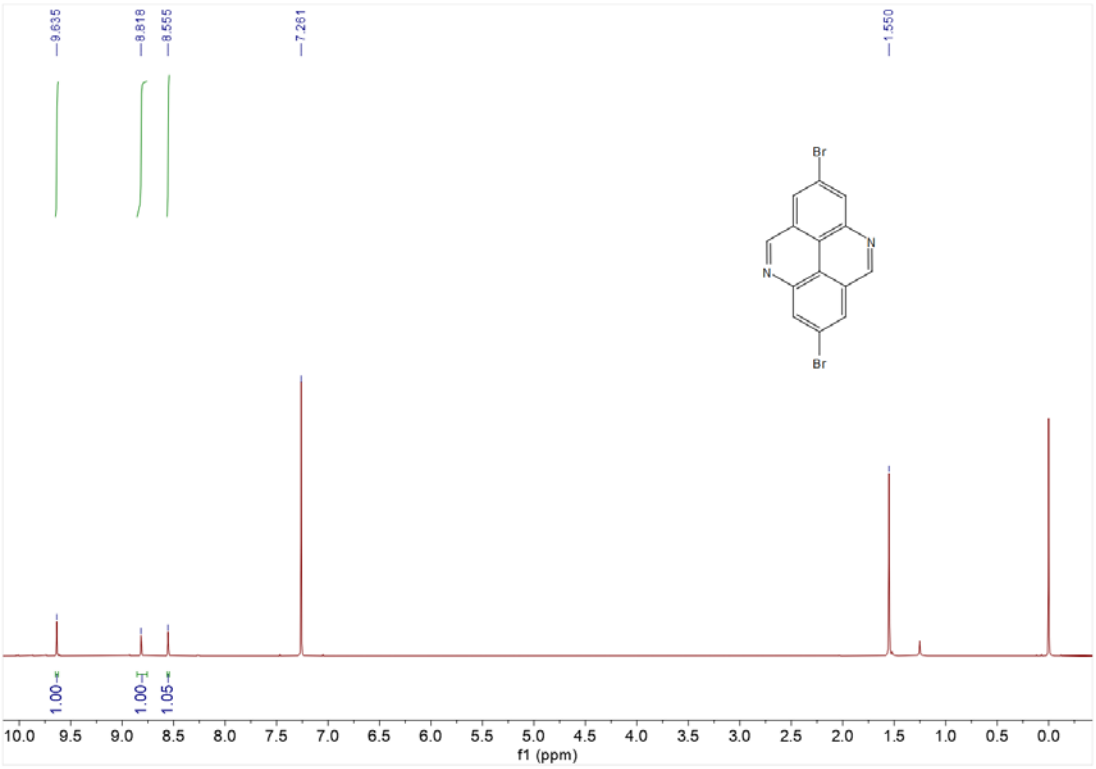

Figure S13. ^{1}H NMR spectrum of **10**.

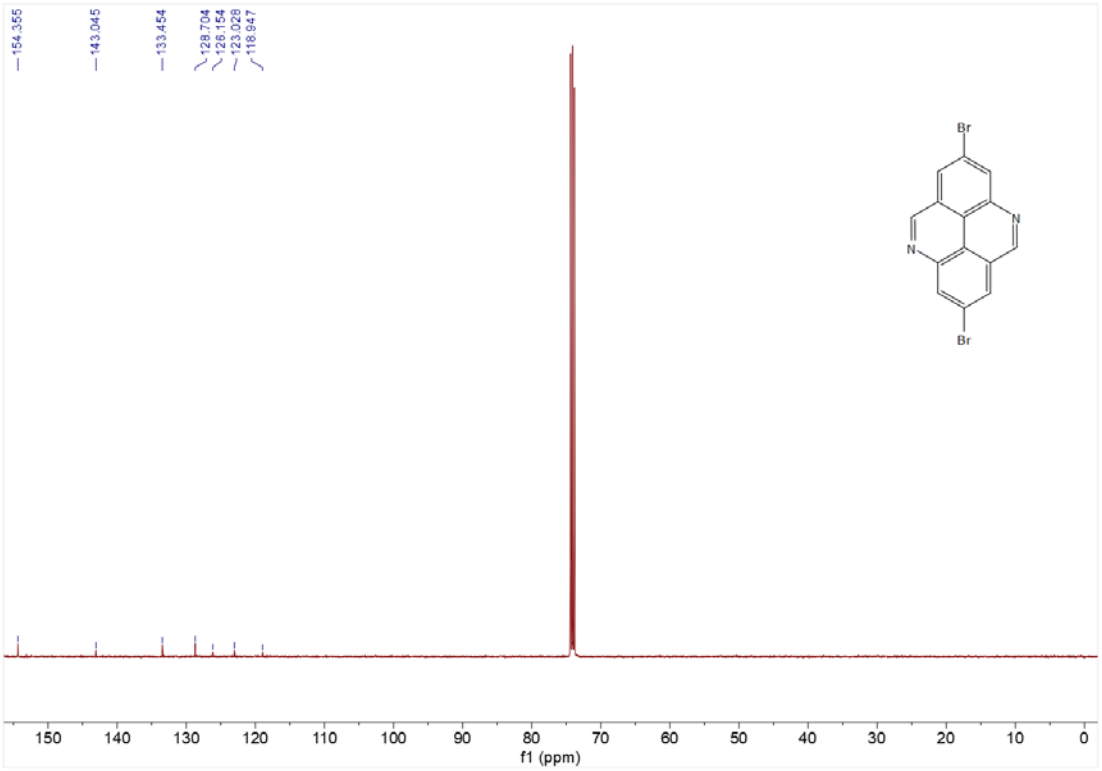

Figure S14. ^{13}C NMR spectrum of **10**.

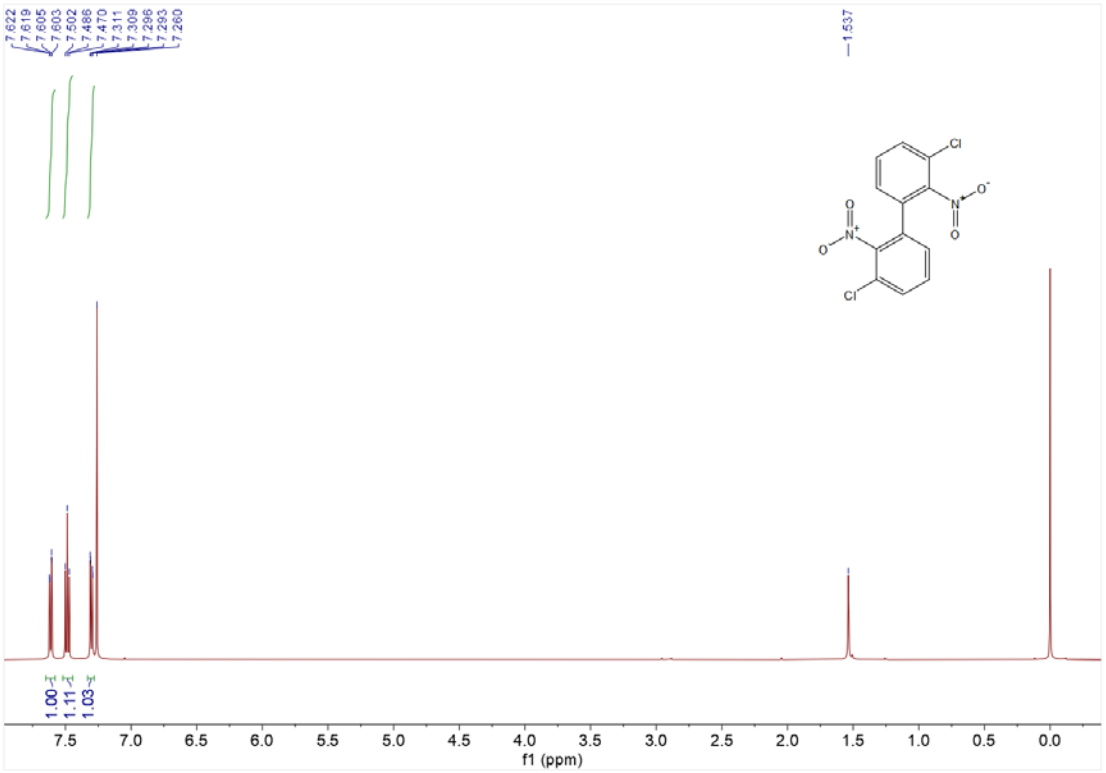

Figure S15. ^{1}H NMR spectrum of **12**.

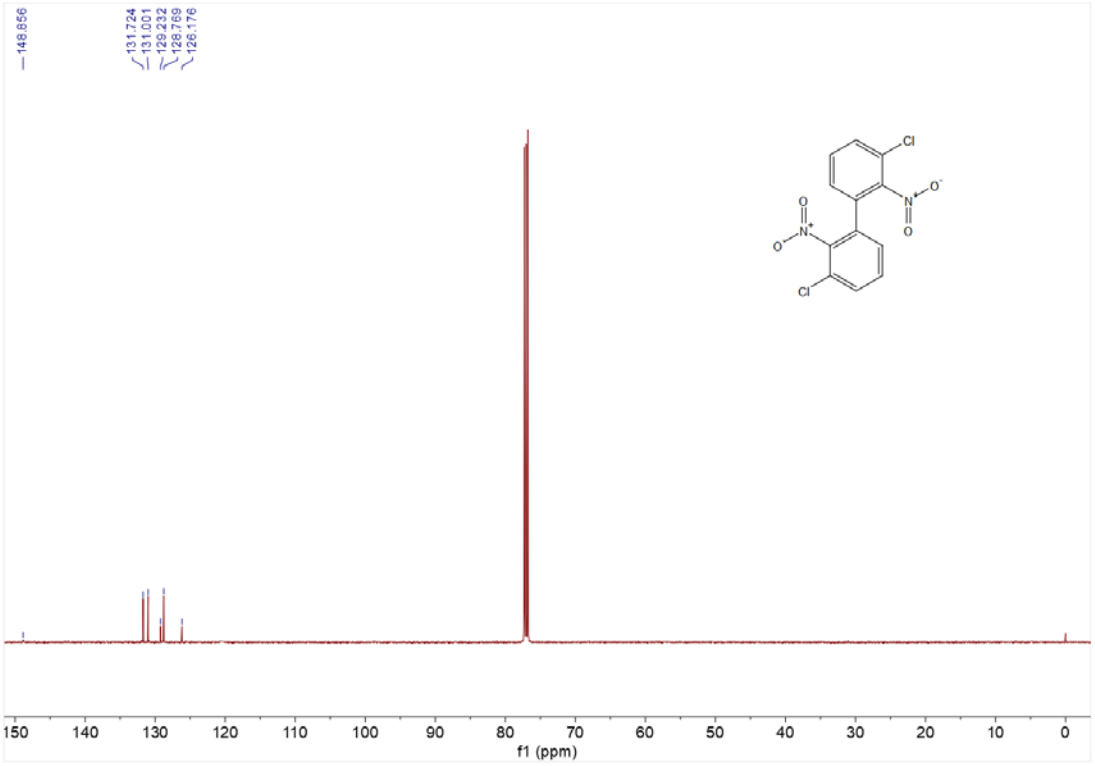

Figure S16. ^{13}C NMR spectrum of **12**.

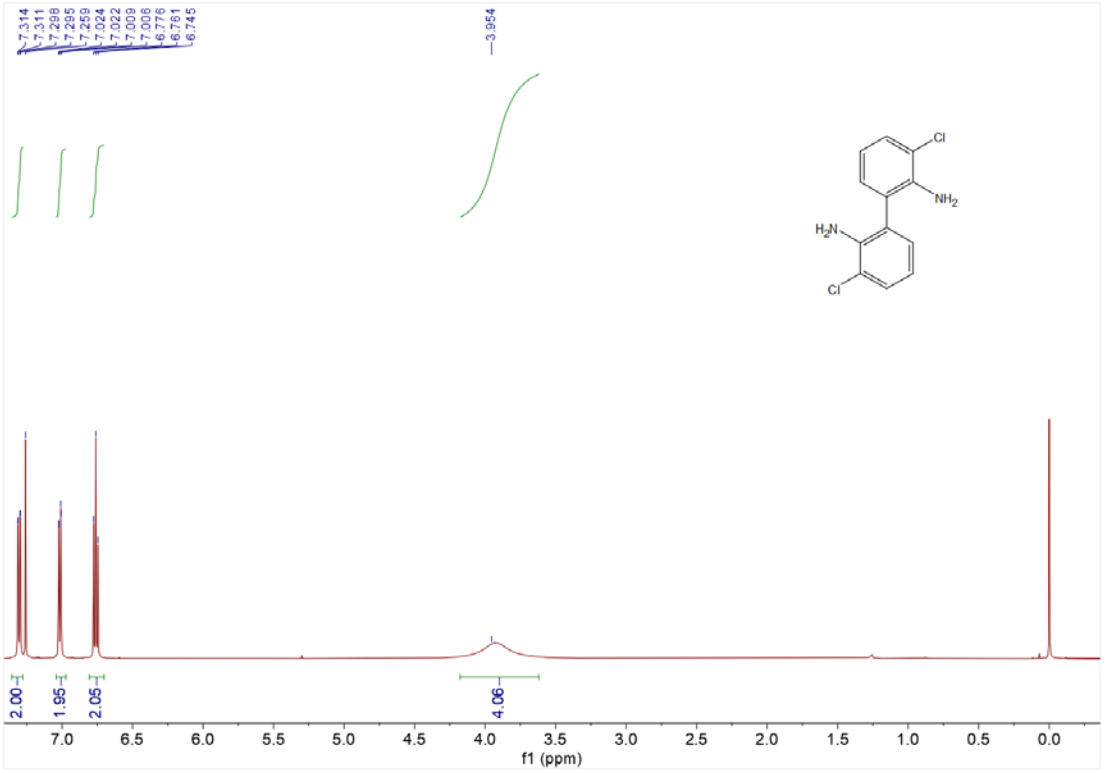

Figure S17. ^{1}H NMR spectrum of **13**.

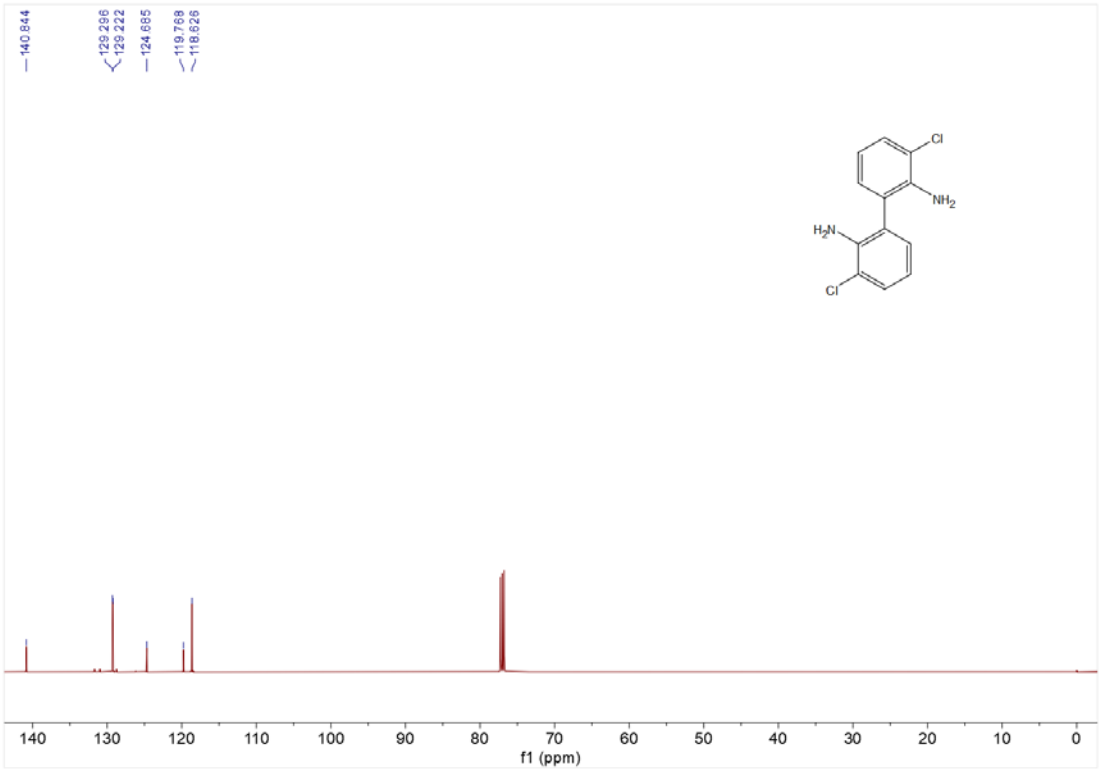

Figure S18. ^{13}C NMR spectrum of **13**.

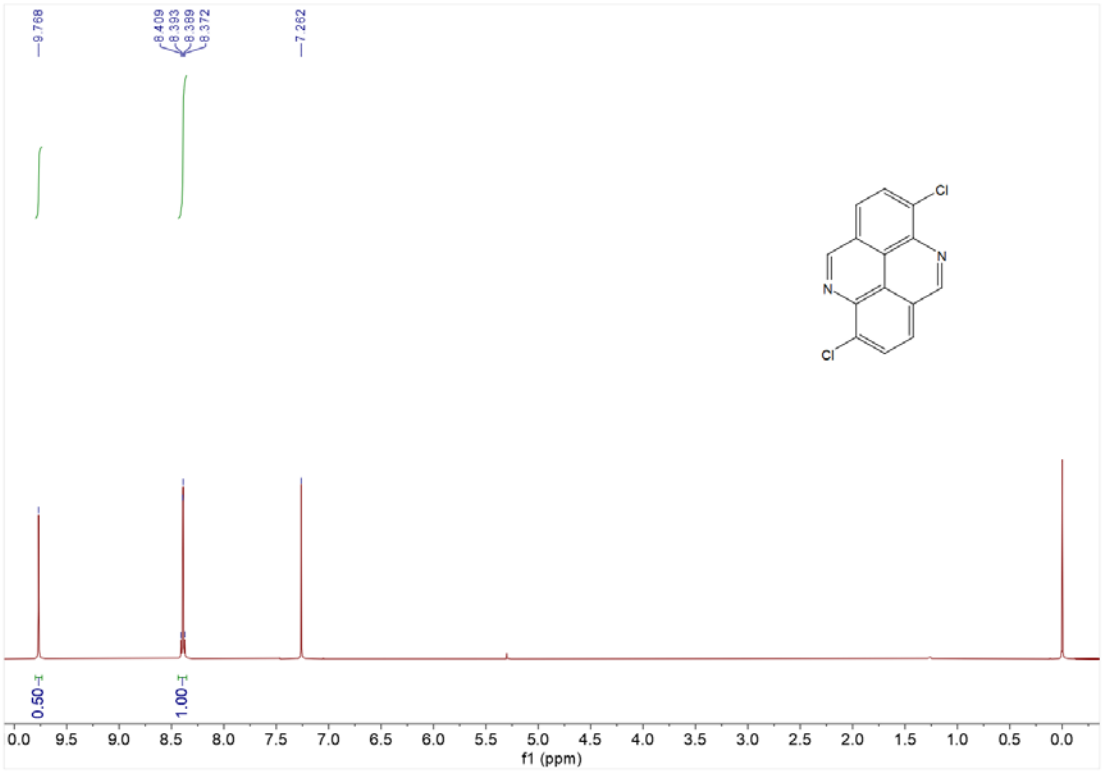

Figure S19. ^{1}H NMR spectrum of **15**.

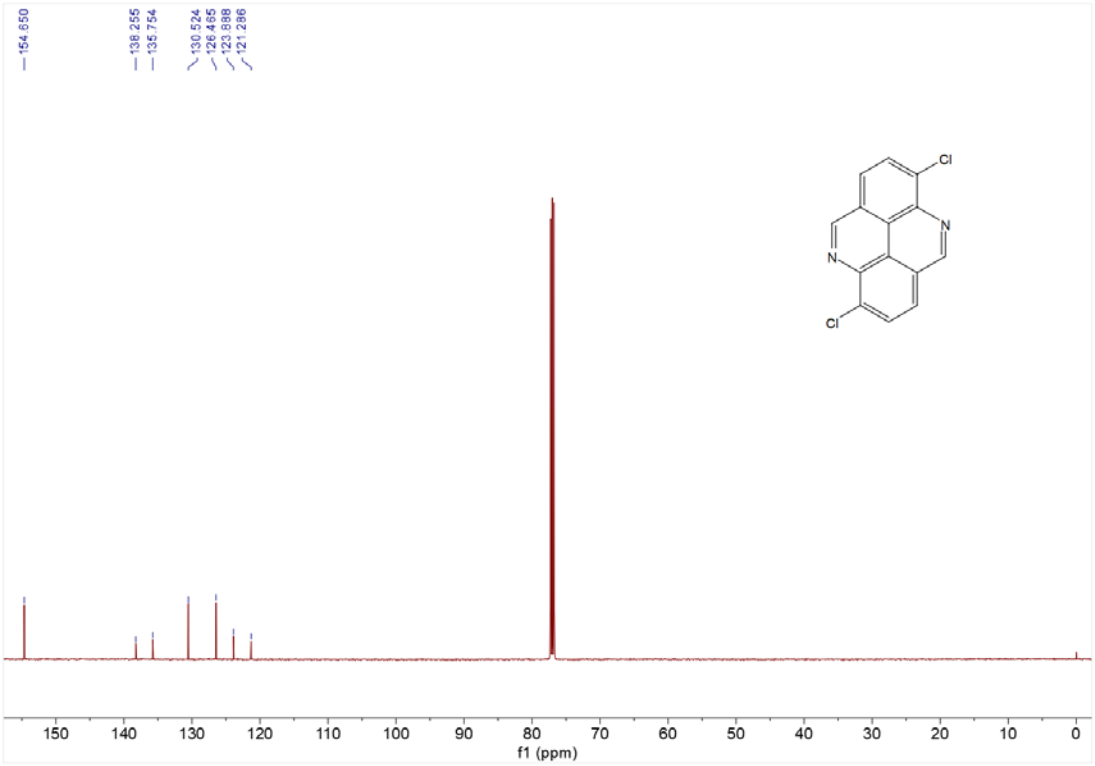

Figure S20. ^{13}C NMR spectrum of **15**.

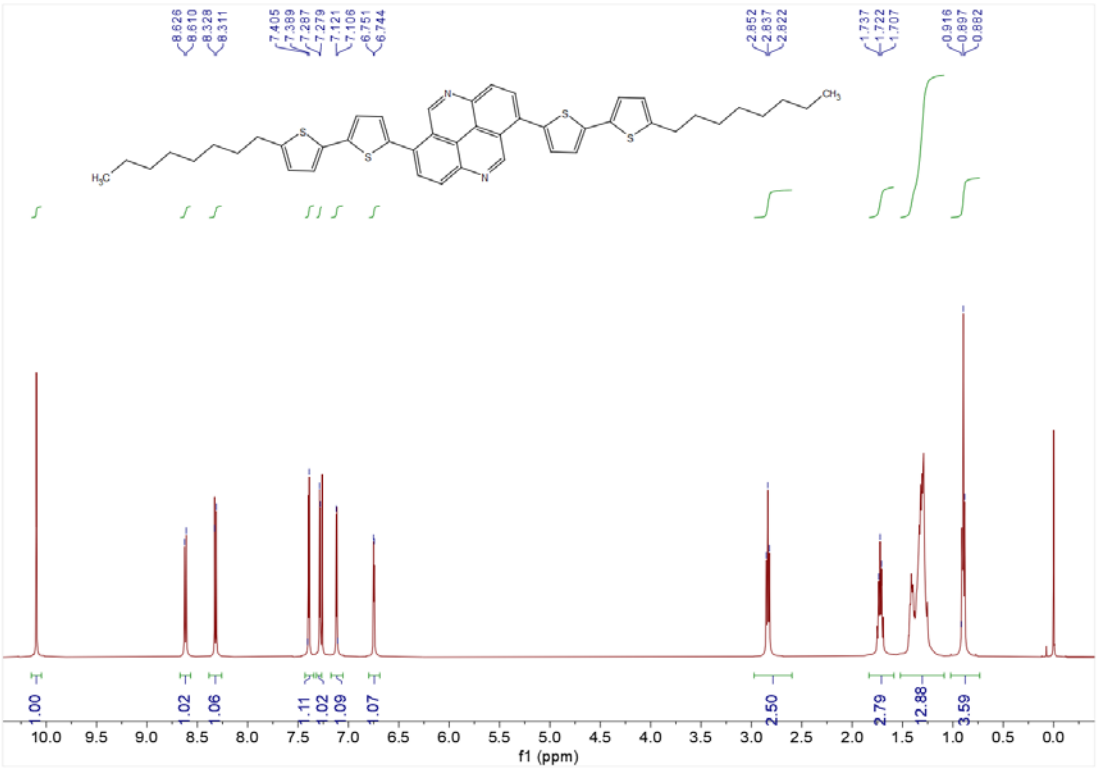

Figure S21. ^{1}H NMR spectrum of **1,6-PyNN-T2**.

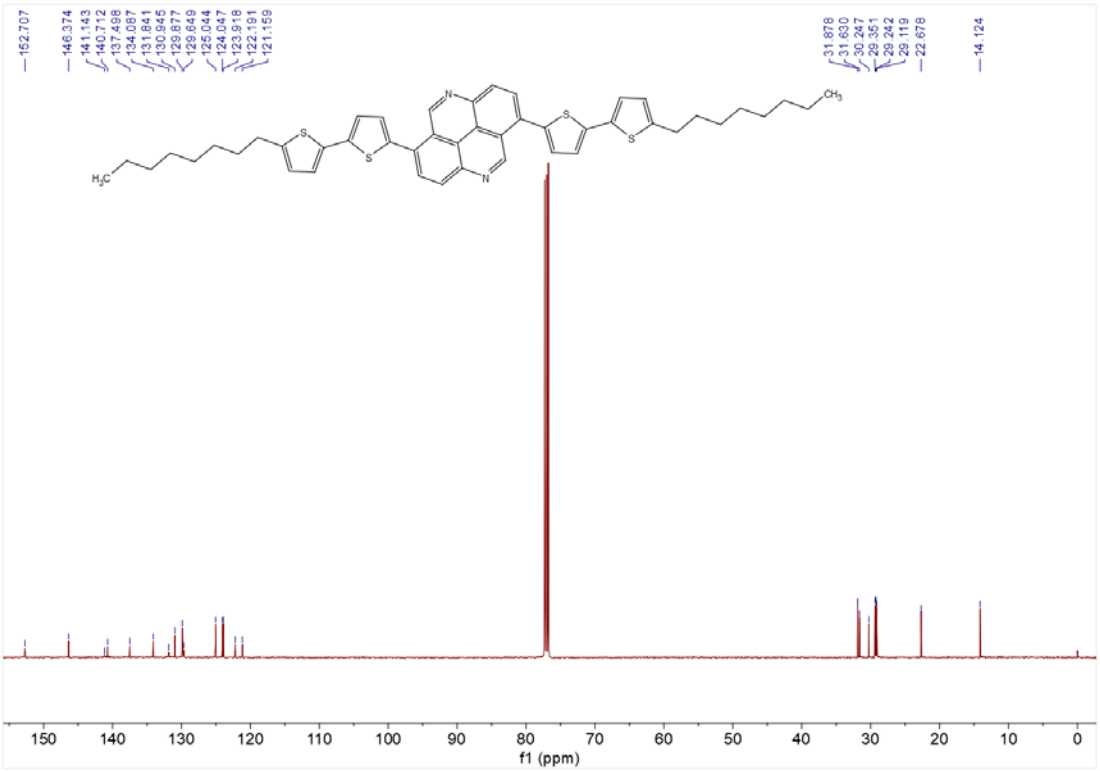

Figure S22. ^{13}C NMR spectrum of **1,6-PyNN-T2**.

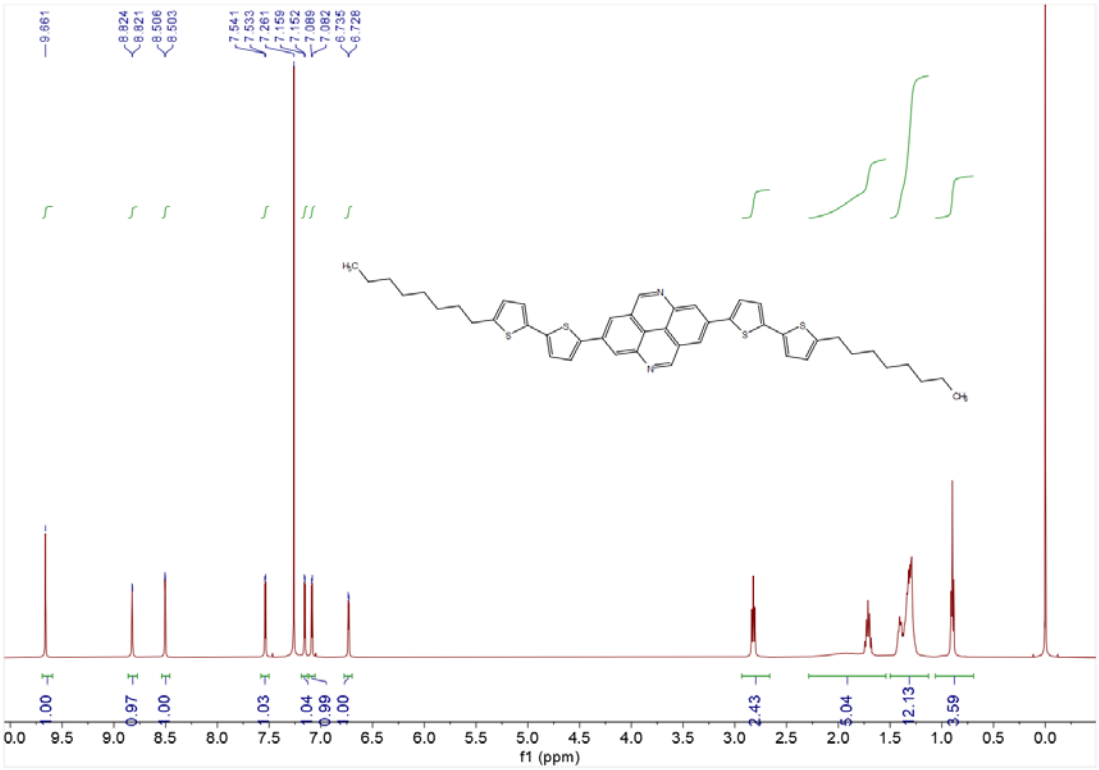

Figure S23. ^{1}H NMR spectrum of **2,7-PyNN-T2**.

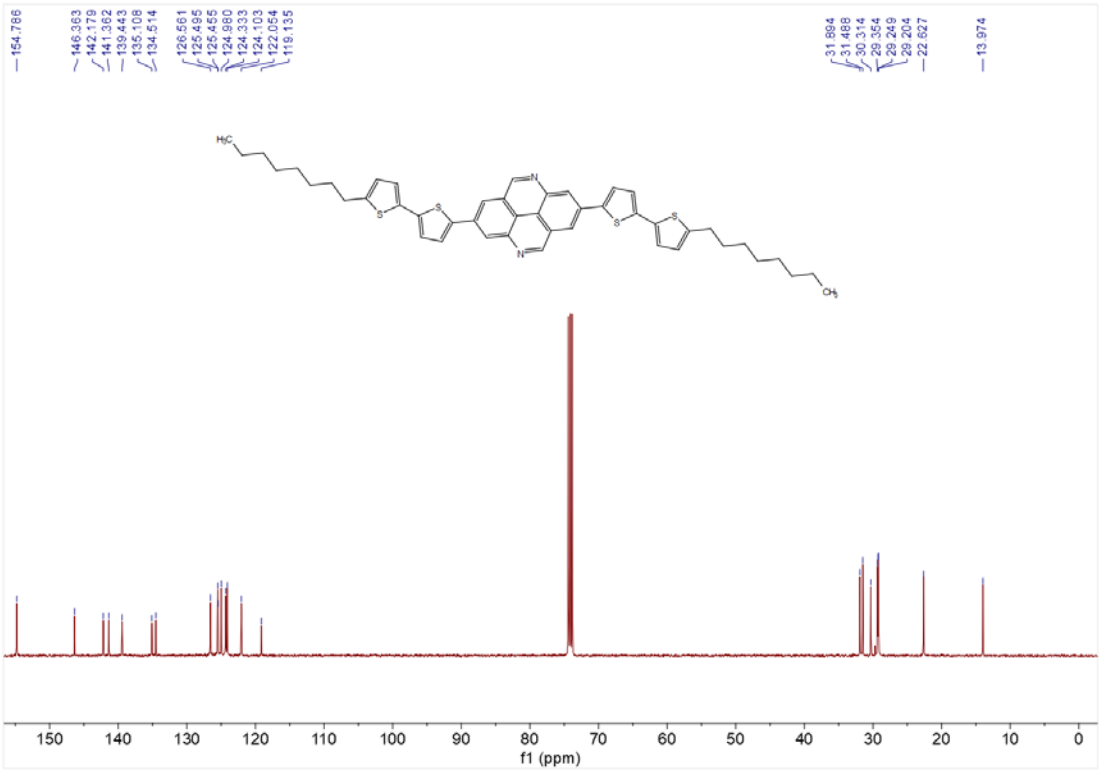

Figure S24. ^{13}C NMR spectrum of **2,7-PyNN-T2**.

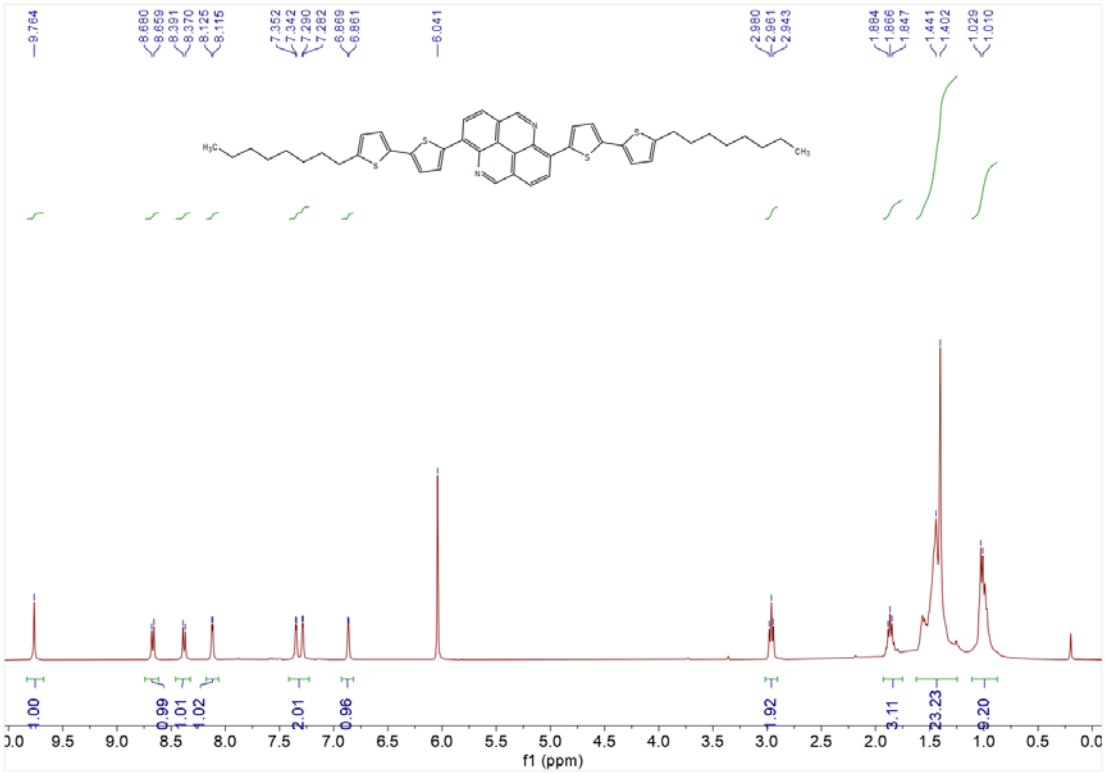

Figure S25. ^{1}H NMR spectrum of **3,8-PyNN-T2**.

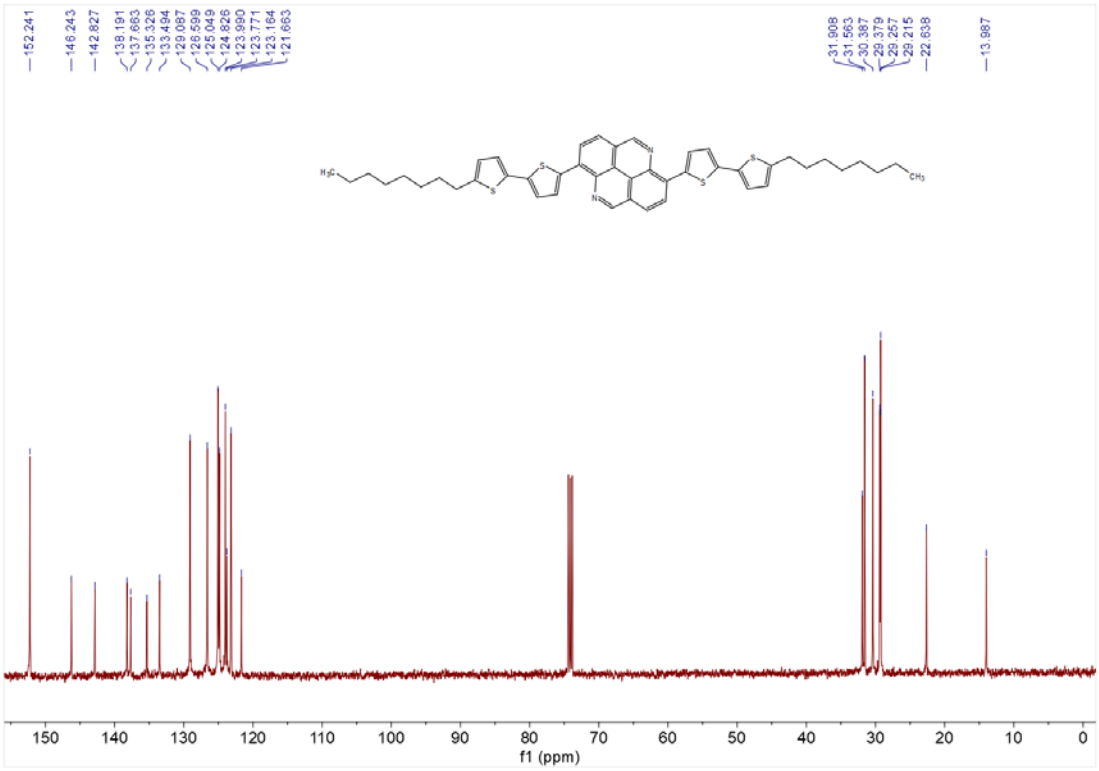

Figure S26. ^{13}C NMR spectrum of **3,8-PyNN-T2**.

4. MALDI-TOF mass spectra

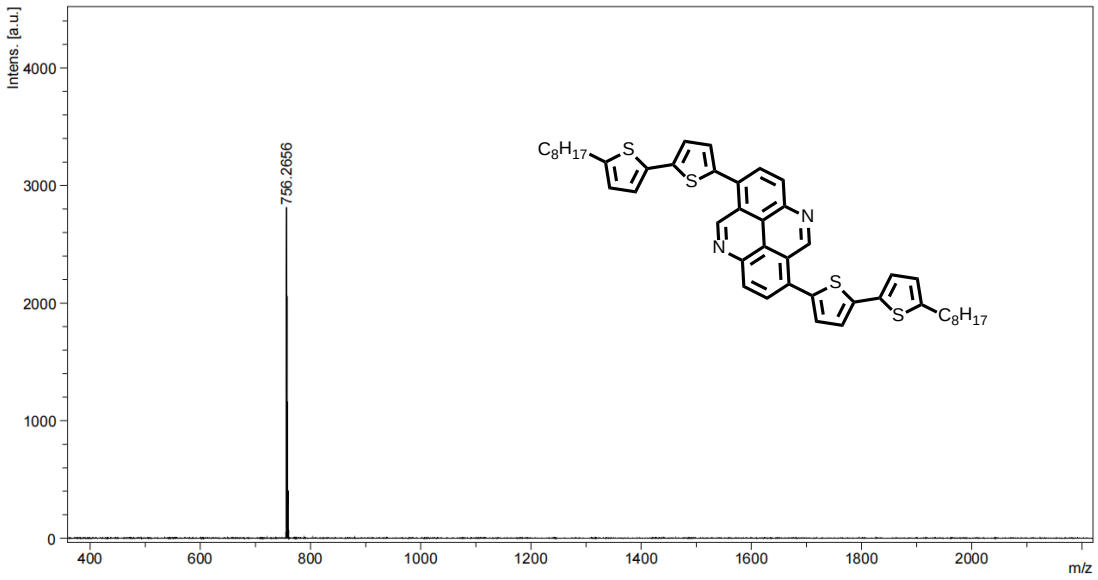

Figure S27. The MALDI-TOF mass spectrum of **1,6-PyNN-T2**.

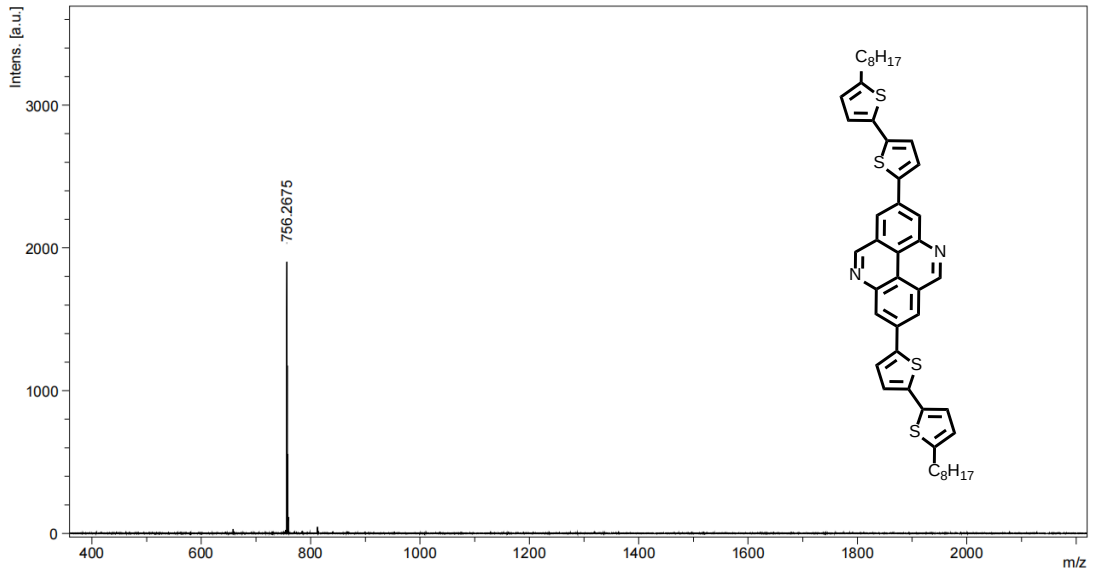

Figure S28. The MALDI-TOF mass spectrum of **2,7-PyNN-T2**.

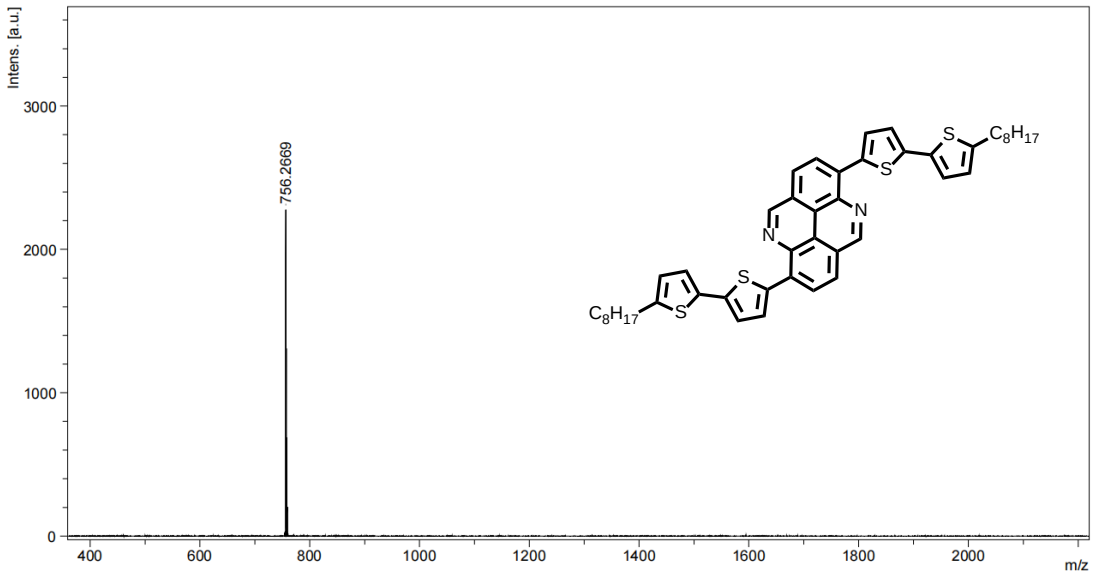

Figure S29. The MALDI-TOF mass spectrum of **3,8-PyNN-T2**.

5. Thermal properties

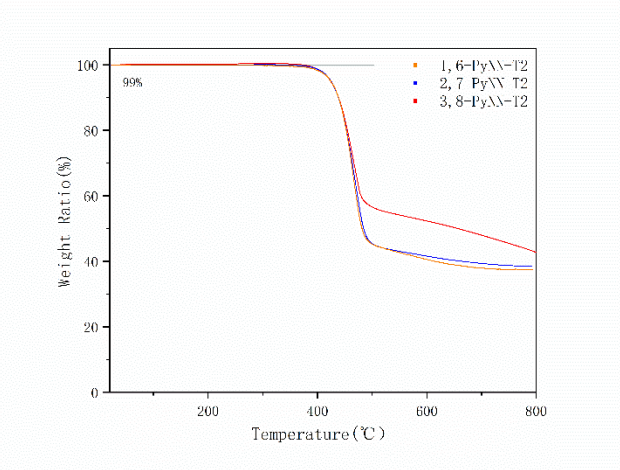

Figure S30. TGA curves of three compounds in N_2 with a heating rate of 10 ^{o}C/min.

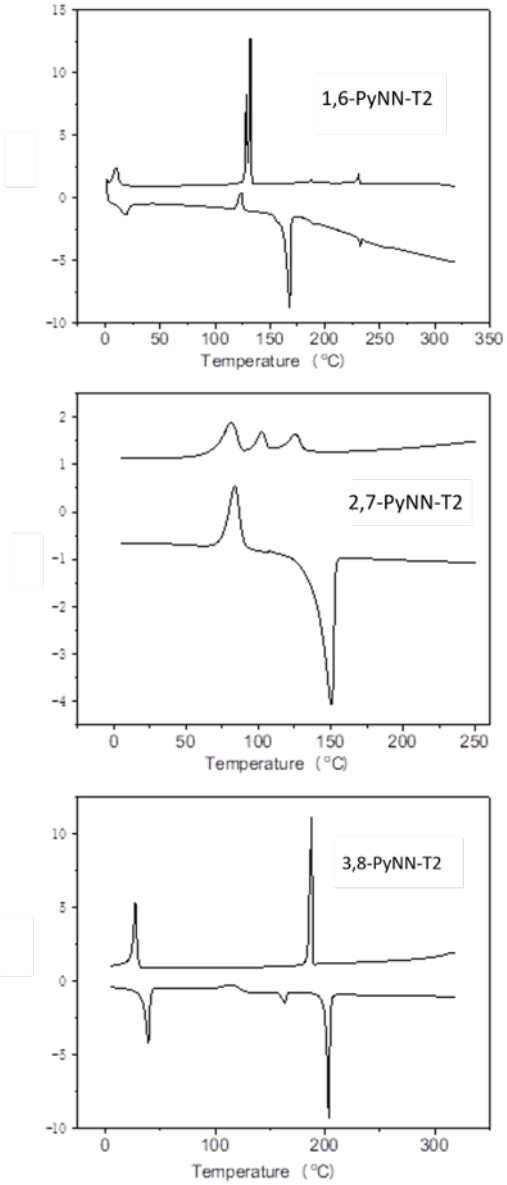

Figure S31. The first cooling and the second heating DSC curves of three compounds in N_2 with a heating/cooling rate of 10 ^{o}C/min.

6. X-ray crystallography

Table S1. Crystal data and structure refinement for **1,6-PyNN-T2 (CCDC: 2371376).**

Identification code	**1,6-PyNN-T2**	
Moiety formula	$C_{46}H_{48}N_2S_4$	
Formula weight	757.10	
Temperature	273 K	
Wavelength	0.71073 Å	
Crystal system	triclinic	
Space group	P-1	
Unit cell dimensions	*a*=6.9434(3) Å	α = 83.743(1) °
	b=8.2926(4) Å	β = 86.710(1) °
	c=34.5873(15) Å	γ = 78.867(3) °
Volume	1941.03(15) $Å^3$	
Z	2	
Density (calculated)	1.295 mg/m^3	
Absorption coefficient	0.281 mm^{-1}	
F(000)	804.0	
Theta range for data collection	2.299 to 26.214°	
Index ranges	$-8 \leq h \leq 8, -10 \leq k \leq 10, -43 \leq l \leq 43$	
Reflections collected	26470	
Independent reflections	7415 [R_{int} = 0.0218]	
Completeness to theta= 27.110°	0.864	
Absorption correction	MULTI-SCAN	
Max. and min. transmission	0.745 and 0.674	
Refinement method	Full-matrix least-squares on F^2	
Data / restraints / parameters	7415/1384/590	
Goodness-of-fit on F^2	1.053	
Final R indices [I>2sigma(I)]	R_1 = 0.0517, wR^2 = 0.1503	
R indices (all data)	R_1 = 0.0568, wR^2 = 0.1566	
Largest diff. peak and hole	0.558 and -0.413 $e.Å^{-3}$	

Table S2. Crystal data and structure refinement for **2,7-PyNN-T2 (CCDC: 2371524).**

Identification code	**2,7-PyNN-T2**
Moiety formula	$C_{46}H_{48}N_2S_4$
Formula weight	757.10
Temperature	173 K
Wavelength	0.71073 Å
Crystal system	monoclinic

Space group	P 2_1/n	
Unit cell dimensions	*a* = 5.5886(3) Å	α = 90°
	b = 7.7122(3) Å	B = 91.274(2)°
	c = 44.122(2) Å	γ = 90°
Volume	1901.19(16) Å^3	
Z	4	
Density (calculated)	1.323 mg/m^3	
Absorption coefficient	0.287 mm^{-1}	
F(000)	804.0	
Theta range for data collection	2.681 to 30.083°	
Index ranges	-7 ≤ h ≤ 7, -10 ≤ k ≤ 10, -62 ≤ l ≤ 62	
Reflections collected	47939	
Independent reflections	5569 [R(int) = 0.0800]	
Completeness to theta= 27.110°	0.999	
Max. and min. transmission	0.972 and 0.966	
Refinement method	Full-matrix least-squares on F^2	
Data / restraints / parameters	5569/1/236	
Goodness-of-fit on F^2	1.087	
Final R indices [I>2sigma(I)]	R_1 = 0.0666, wR^2 = 0.1557	
R indices (all data)	R_1 = 0.1002, wR^2 = 0.1747	
Largest diff. peak and hole	0.839 and -0.847 e.Å^{-3}	

Table S3. Crystal data and structure refinement for **3,8-PyNN-T2 (CCDC: 2371380).**

Identification code	**3,8-PyNN-T2**	
Moiety formula	$C_{46}H_{48}N_2S_4$	
Formula weight	757.10	
Temperature	273.15	
Wavelength	0.68883 Å	
Crystal system	monoclinic	
Space group	C/c	
Unit cell dimensions	*a* = 10.673(2) Å	α = 90°
	b = 10.506(2) Å	β = 92.061(4)°
	c = 67.260(13) Å	γ = 90°
Volume	7537(2) Å^3	
Z	4	
Density (calculated)	1.334 mg/m^3	
Absorption coefficient	0.268 mm^{-1}	
F(000)	3216	
Theta range for data collection	1.174 to 24.219°	
Index ranges	-12 ≤ h ≤ 12, -11 ≤ k ≤ 11, -80 ≤ l ≤ 80	
Reflections collected	24019	
Independent reflections	10004 [R_{int} = 0.1169]	

Completeness to theta= 27.110°	0.799
Max. and min. transmission	0.7450 and 0.4160
Refinement method	Full-matrix least-squares on F^2
Data / restraints / parameters	10004/4004/943
Goodness-of-fit on F^2	1.101
Final R indices [I>2sigma(I)]	R_1 = 0.1225, wR^2 = 0.3089
R indices (all data)	R_1 = 0.1715, wR^2 = 0.3523
Largest diff. peak and hole	0.467 and -1.136 e.$Å^{-3}$

7. OFET devices performances

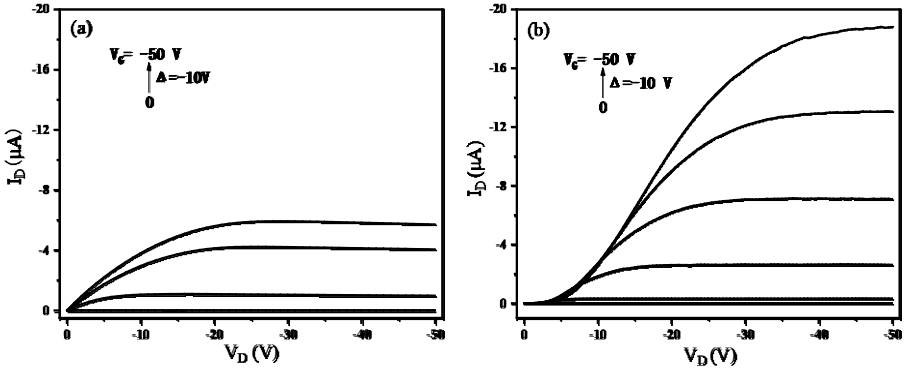

Figure S32. Typical output characteristics of OFET with vacuum deposited 3,8-PyNN-T2 film (a) and single-crystal (b). The nonlinear current increase in the low V_D regime in (b) indicative the crystals have bigger thickness.

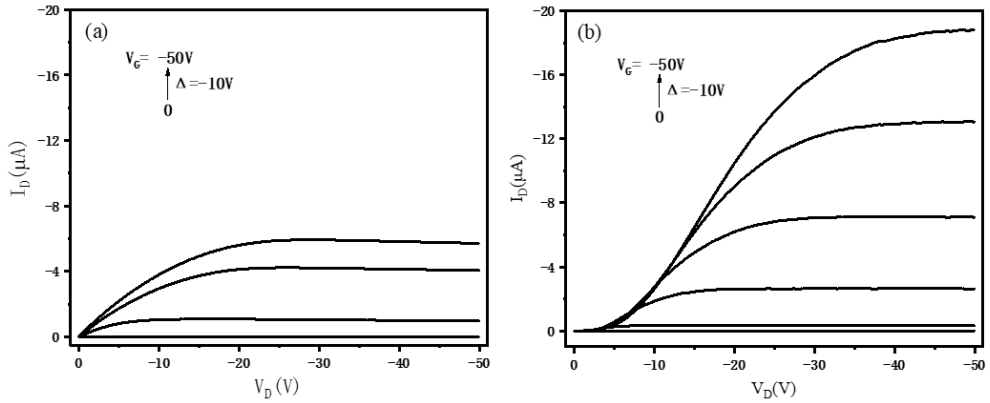

Table S4. OTFT device performance of 3,8-PyNN-T2 at different substrate deposition temperatures. All devices were measured in air.

	T_s (°C)	μ ($cm^2V^{-1}s^{-1}$)	V_{th} (V)	I_{on}/I_{off}
3,8-PyNN-T2	25	0.09-0.13	-10 to -17	10^5-10^6
	90	0.15-0.17	-7 to -8	10^5-10^6
	120	0.09-0.10	-15 to -16	10^5-10^6

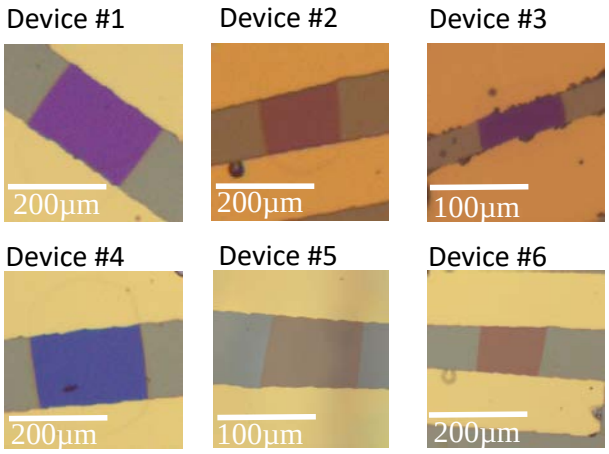

Figure S33. The optical pictures of six single crystal OFETs devices.

Table S5. Channel dimension and mobilities of single crystal OFETs device of 3,8-PyNN-T2.

Device number	Wide (μm)	Length ((μm))	W/L	μ ($cm^2V^{-1}s^{-1}$)
#1	227	150	1.5	1.14
#2	147	114	1.3	0.91
#3	86	32	1.7	0.62
#4	224	147	1.5	1.03
#5	91	64	1.4	0.82
#6	124	70	1.8	0.70
				0.86[a]

[a] the average mobility of single crystal OFETs devices.

8. Film morphology

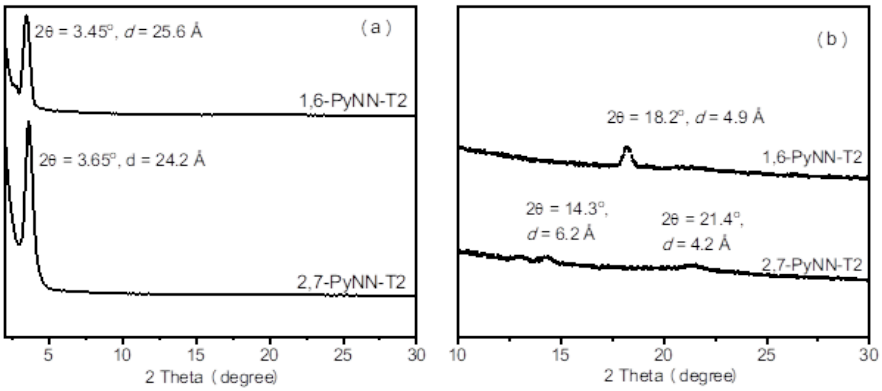

Figure S34. Out-of-plane (a) and in-plane (b) X-ray diffraction (XRD) patterns of 1,6-PyNN-T2 and 2,7-PyNN-T2 thin film prepared by vacuum deposition. Compared to the single crystal diffraction data of 1,6- and 2,7-PyNN-T2 obtained from table S1-S3, the peaks illustrated in (a) and (b) cannot be assigned, indicating the packing structures of both molecules in the films were different from those in the single crystals, which may have a negative impact on the charge carries transfer.

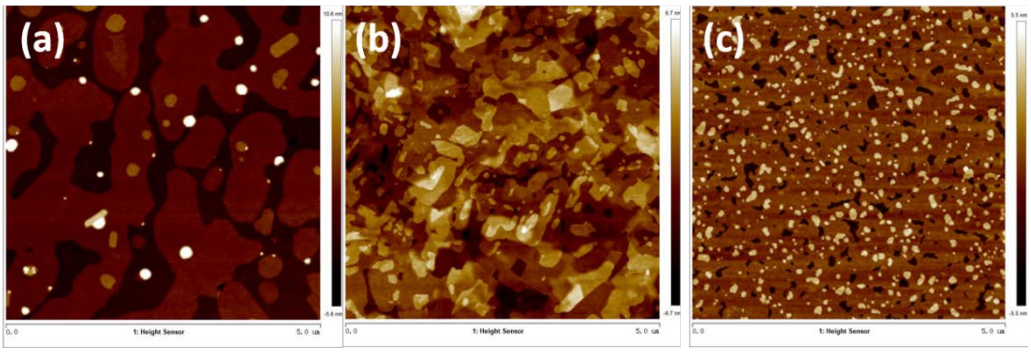

Figure S35. AFM height images (5 x 5 μm^2) of the thin films of 1,6-PyNN-T2 (a), 2,7-PyNN-T2 (b) and 3,8-PyNN-T2 (c) with thickness of 30 nm deposited on Sub_{OTMS}.

9. References

1. Gaussian 09 (Revision A.02), M. J. Frisch, G. W. Trucks, H. B. Schlegel, G. E. Scuseria, M. A. Robb, J. R. Cheeseman, G. Scalmani, V. Barone, B. Mennucci, G. A. Petersson, H. Nakatsuji, M. Caricato, X. Li, H. P. Hratchian, A. F. Izmaylov, J. Bloino, G. Zheng, J. L. Sonnenberg, M. Hada, M. Ehara, K.

Toyota, R. Fukuda, J. Hasegawa, M. Ishida, T. Nakajima, Y. Honda, O. Kitao, H. Nakai, T. Vreven, J. A. Montgomery, Jr., J. E. Peralta, F. Ogliaro, M. Bearpark, J. J. Heyd, E. Brothers, K. N. Kudin, V. N. Staroverov, R. Kobayashi, J. Normand, K. Raghavachari, A. Rendell, J. C. Burant, S. S. Iyengar, J. Tomasi, M. Cossi, N. Rega, J. M. Millam, M. Klene, J. E. Knox, J. B. Cross, V. Bakken, C. Adamo, J. Jaramillo, R. Gomperts, R. E. Stratmann, O. Yazyev, A. J. Austin, R. Cammi, C. Pomelli, J. W. Ochterski, R. L. Martin, K. Morokuma, V. G. Zakrzewski, G. A. Voth, P. Salvador, J. J. Dannenberg, S. Dapprich, A. D. Daniels, Ö. Farkas, J. B. Foresman, J. V. Ortiz, J. Cioslowski, D. J. Fox, Gaussian, Inc., Wallingford CT, 2009.

2. E. F. Valeev, V. Coropceanu, D. A. da Silva Filho, S. Salman and J.-L. Brédas, Effect of Electronic Polarization on Charge-Transport Parameters in Molecular Organic Semiconductors. *J. Am. Chem. Soc.* 2006, **128**, 9882−9886.
3. J. S. Huang and M. Kertesz, Intermolecular Transfer Integrals for Organic Molecular Materials: Can Basis Set Convergence Be Achieved? Chem. Phys. Lett. 2004, 390, 110-115.
4. X. D.Yang, L. J. Wang, C. L.Wang, W. Long and Z. G.Shuai, Influences of Crystal Structures and Molecular Sizes on the Charge Mobility of Organic Semiconductors: Oligothiophenes. Chem. Mater. 2008, 20, 3205-3211.
5. D. M. Takeo Sasaki, Komei Akaike, Masashi Ikegamia and Yumiko Naka, Photorefractive Effect of Photoconductive Ferroelectric Liquid Crystalline Mixtures Composed of Photoconductive Chiral Compounds and Liquid Crystal, *J. Mater. Chem.*, 2011, **21**, 8678-8686.
6. L. Liang, J.-T. Wang, X. Xiang, J. Ling, F.-G. Zhao and W.-S. Li, Influence of Moiety Sequence on the Performance of Small Molecular Photovoltaic Materials, *J. Mater. Chem. A*, 2014, **2**, 15396-15405.
7. C. Y. Chen, S. J. Wu, C. G. Wu, J. G. Chen and K. C. Ho, A Ruthenium Complex with Superhigh Light-Harvesting Capacity for Dye-Sensitized Solar Cells, *Angew. Chem. Int. Ed.*, 2006, **45**, 5822-5825.
8. E. A. T. Sergei A. Ponomarenko, Aziz M. Muzafarov, Stephan Kirchmeyer, Lutz Brassat, Ahmed Mourran, Martin Moeller, Sepas Setayesh, and Dago de Leeuw, Star-Shaped Oligothiophenes for Solution-Processible Organic Electronics: Flexible Aliphatic Spacers Approach, *Chem. Mater.*, 2006, **18**, 4101-4108.
9. A. A. V. Yutaka Ito, Stefan Mannsfeld, Joon Hak Oh, Michael Toney,Jason Locklin, and Zhenan Bao, Crystalline Ultrasmooth Self-Assembled Monolayers of Alkylsilanes for Organic Field-Effect Transistors, *J. Am. Chem. Soc.*, 2009, **131**, 9396–9404.
10. H. Klaasen, L. Liu, H.-Y. Gao, L. Viergutz, P. A. Held, T. Knecht, X. Meng, M. C. Börner, D. Barton, S. Amirjalayer, J. Neugebauer, A. Studer and H. Fuchs, Intermolecular Coupling and Intramolecular Cyclization of Aryl Nitriles on Au(111), *Chem. Commun.*, 2019, **55**, 11611-11614.
11. I. R. K. m. A. I. Tochilkin, E. P. Prokof'ev, I. N. Gracheva, and M. V. Levinskii, Bromination of Quinoline Derivatives with N-bromosuccinmide. Isomeric

Composition of the Bromination Products by Pmr and Glc, *Chem. Heterocycl. Compd.*, 1989, **24**, 892–897.

12. Y. Han, Z. Hu, M. Liu, M. Li, T. Wang and Y. Chen, Synthesis, Characterization, and Properties of Diazapyrenes via Bischler-Napieralski Reaction, *J. Org. Chem.*, 2019, **84**, 3953-3959.
13. M. H.-S. a. H. Sharghi, ZnO as a New Catalyst for N-Formylation of Amines under Solvent-Free Conditions, *J. Org. Chem.*, 2006, **71**, 6652-6654.
14. J. Cornella, H. Lahlali and I. Larrosa, Decarboxylative Homocoupling of (Hetero)aromatic Carboxylic Acids, *Chem. Commun.*, 2010, **46**, 8276–8278.